Divergent Protein Kinase A contributes to the regulation of flagellar waveform of the motile flagellum of *Leishmania mexicana*

Running Head: PKA modulates flagellar waveforms in *Leishmania*

Authors

Sophia Fochler [1, 2], Benjamin J Walker[3],[4], Richard John Wheeler [5], Eva Gluenz [2, 6]

Affiliations

[1] Sir William Dunn School of Pathology, University of Oxford, Oxford, UK

[2] Institute of Cell Biology, University of Bern, Switzerland

[3] Department of Mathematical Sciences, University of Bath, Bath, UK

[4] Department of Mathematics, University College London, London, UK

[5] Medawar Building for Pathogen Research, Nuffield Department of Medicine, University of Oxford, Oxford, UK.

[6] Wellcome Centre for Integrative Parasitology, School of Infection and Immunity, University of Glasgow

* To whom correspondence should be addressed: eva.gluenz@unibe.ch

Abstract

Protein kinase A (PKA) is one of the most studied eukaryotic signal transducers and a key target of the second messenger cAMP. Kinetoplastids, a branch of early diverging eukaryotes, possess homologues of catalytic and regulatory PKA subunits that, unusually, are insensitive to cAMP with uncertainty about the endogenous activating ligand. While previous evidence has implicated both cAMP and PKA in the regulation of flagellar motility in kinetoplastids, the specific contributions of the two regulatory (PKAR) and three catalytic (PKAC) subunits of PKA remain unclear. Here we conducted a systematic study combining reverse genetics and microscopy analysis to investigate PKAC and PKAR subcellular localisations, pairing preferences, and the effect of PKA gene deletions on swimming speed and flagellar waveforms in *Leishmania mexicana* promastigotes. *Lmx*PKAC1, *Lmx*PKAC2 and *Lmx*PKAR1 are enriched in the flagellum and upon detergent extraction, the *Lmx*PKAR1 and *Lmx*PKAC1 signals remained associated with the cytoskeleton. The flagellar *Lmx*PKAC1 and *Lmx*PKAC2

signals were, however, greatly diminished by removal of *Lmx*PKAR1, consistent with an anchoring function for the R-subunit. Previous work identified the *Streptomyces* antimetabolite toyocamycin, activated the divergent PKA of *Trypanosoma brucei*. The patterns of sequence divergence within the phosphate binding cassettes of *Lmx*PKAR1 and *Lmx*PKAR3 suggest both are divergent from *T. brucei*. We therefore tested the effect of toyocamycin and a similarly structured compound of the purine metabolism pathway, inosine, on the localisation of *Lmx*PKAC1 and found that the *Lmx*PKAC1 mNG signal was lost from the cytoskeletal fraction following treatment with either toyocamycin or inosine. *Lmx*PKAC3 and *Lmx*PKAR3 were localised to the cell cortex. Upon removal of *Lmx*PKAR3, *Lmx*PKAC3 was lost from the cortex and became distributed throughout the cell, including an increased presence in the flagellum. Assessing motility phenotypes, we found this increase of *Lmx*PKAC3 signal in the flagellum correlated with an increase in swimming speed. Whereas the deletion of *Lmx*PKAC3 resulted in flagella beating at significantly reduced frequencies and a resulting decrease in population swimming speed. Moreover, *Lmx*PKAC1 null mutants showed a significantly reduced swimming speed and cells were unable to produce symmetric flagellar waves. Taken together these data indicate that the divergent PKA pathway in *Leishmania* modulates flagellar motility.

Author Summary

Many cells use whip-like cellular appendages, called flagella, for swimming. Regulating the rhythm and strength of the flagellar beat is important to determine the speed at which cells swim and in what direction they move. How this regulation is accomplished is not fully understood. Here we examined the role of protein kinase A (PKA) in flagellar motility of the unicellular parasite Leishmania. Leishmania have three catalytic PKA proteins, which transduce upstream signals through protein phosphorylation, and two regulatory PKA proteins that serve to anchor the catalytic subunits to specific locations within the cell. We show that two catalytic and one regulatory subunit are part of the flagellar cytoskeleton, while the other regulatory subunit docks its catalytic subunit to the cytoskeleton surrounding the cell body. Removal of individual PKA proteins perturbed the flagellar beat in different ways. We found that cells that lacked the catalytic subunit PKAC1 could only beat their flagella in an uncoordinated manner and as a consequence swam more slowly. These findings suggest that Leishmania PKA proteins are part of a pathway that regulates flagellar beating.

Introduction

Motile cilia and flagella are dynamic specialised organelles comprised of soluble, membrane-associated and cytoskeletal components. Over 700 proteins (1–4) form the microtubule axoneme, which typically consists of nine outer doublet microtubules and two central singlet microtubules (called the central pair, CP). Radial spoke complexes (RS) project from the outer doublets to the CP and nexin linkages connect adjacent doublets radially. Two rows of dynein motor protein complexes, the outer dynein arms (ODA) and inner dynein arms (IDA), are studded with 96 nm periodicity along the outer doublet microtubules (5). Dyneins are part of a family of ATPases which hydrolyse ATP in order to iteratively bind, pull and release along adjacent microtubule structures (6). This sliding is converted to bending via the sliding restrictions imposed by basal body anchoring and inter-microtubule nexin linkages (7) While eukaryotic flagella generally rely on the same fundamental mechanism and a set of conserved core structures and protein complexes, important open questions still remain about how flagellar beats are propagated and modulated. Moreover, little is known of how different types of cells translate specific cues from the local environment into appropriate flagellar beating patterns.

Calcium and cAMP are the two main second messengers that have been linked to changes in flagellar beating behaviours in diverse types of cilia and flagella, including mammalian respiratory cilia (8), human sperm (9,10) bull sperm (11,12), hamster sperm (13,14) and sea urchin sperm (15–17), the green algae *Chlamydomonas* (18–20), *Paramecium* (21,22), Euglena (23) and *Leishmania* (24,25).

Increases in intraciliary cAMP concentration have been observed to correlate with increased beat frequency in mammalian cilia (26,27). The second messenger signal is transmitted through kinases, phosphatases and calcium-binding proteins that are thought to be incorporated into core axoneme structures (17,28–31). A key transducer of cAMP signals is cAMP-dependent protein kinase (PKA), a highly conserved protein of the AGC kinase subgroup, owing to its similarities to cGMP-dependent protein kinase (PKG) and protein kinase C (PKC) (16). The paradigm for eukaryotic PKA signal transduction involves a heterotetrameric holoenzyme composed of two PKA catalytic subunit (PKAC) and two PKA regulatory subunit (PKAR), (C_2R_2). In its inactive state, unbound to cAMP, the autoinhibitory domain (AI) of PKAR occupies and inhibits the catalytic core of the PKAC subunit (33). Upon binding of two cAMP molecules to each of the PKAR subunits, the PKAC is then released to phosphorylate its substrates. In vertebrates, A-kinase anchoring proteins (AKAPs) bind the PKA heterotetrameric

93 holoenzyme via the RII domains in the PKAR, creating local micro-signalosomes (34).
94 Flagellar ODAs are thought to represent an important target of PKA (35,36).
95 Flagellate protozoa of the genera *Leishmania* and *Trypanosoma* are well-studied due to their
96 importance as parasites of humans and livestock. They also provide genetically tractable study
97 models for eukaryotic flagella in a lineage that is distinct from humans, green algae
98 (*Chlamydomonas*) and ciliates (e.g. *Tetrahymena*, *Paramaecium*). Trypanosomatid signal
99 transduction pathways remain poorly defined and whilst cAMP signalling has been linked to
100 flagellar waveform modulation (24), there is considerable uncertainty how signals are
101 transduced within trypanosomatid flagella.
102 All available kinetoplastid genomes, asides from the aflagellate endosymbiont *Perkinsela*,
103 encode three PKAC genes that share some canonical features of eukaryotic PKAs, such as the
104 conserved phosphoresidue located in the activation loop (37) along with a conserved catalytic
105 core sequence (38). Intriguingly, however it has been established that PKA in trypanosomes
106 forms C_1R_1 heterodimers and does not respond to cAMP (38,39). Instead, analogues of 7-
107 deazaadenosine (tubercidin), including toyocamycin were shown to activate *T. brucei* PKA
108 (TbPKA) by binding TbPKAR. The highest activation and binding activity was shown for the
109 compound 7-cyano-7-deazainosine (7-CN-7-C-Ino) (38), but the identity of the physiological
110 ligand remains to be confirmed. Interestingly, when the known mammalian PKA
111 phosphorylation substrate vasodilator-stimulated protein (VASP) was exogenously expressed
112 in *T. brucei* it was phosphorylated on serine-157 by endogenous parasite PKA (38), suggesting
113 that although *Trypanosoma* PKA homologues are not regulated by cyclic nucleotides, some
114 downstream targets may still be shared across eukaryotic species.
115 Several lines of evidence point towards the trypanosomatid flagellum as a key site for PKA
116 function. First, flagellar localisation has been demonstrated for PKAC1/2 and PKAR subunits,
117 in flagellar proteomes of *T. brucei* and *L. mexicana* (40,41), by labelling *L. donovani*
118 promastigote forms and *T. brucei* with PKAR1-specific antibodies (42) and in protein tagging
119 screens (41,43,44). Moreover, the flagellar localisation of TbPKAR1 was shown to depend on
120 IFT (45). Second, loss-of-function mutations altered parasite motility patterns: Depletion of
121 TbPKAR1 by RNAi in bloodstream forms reduced the cells' capacity for forward motility (40).
122 Knockout of PKAR1 or a partial deletion of PKAC1 slowed the swimming speeds of *L.*
123 *mexicana* promastigotes (41). Finally, the developmental regulation of transcripts and activity
124 in *Leishmania* spp. reflects the presence or absence of a motile flagellum: *L. major*
125 promastigotes, which possess a motile flagellum showed much higher transcript levels (46)
126 than the amastigote form which only have a short, non-motile cilium (42,47) and proteome-

127 wide the phosphorylation kinetics of the PKA target motif (RXXS*/T*) in *L. donovani* during
128 promastigote to amastigote differentiation consistently detected the highest signal in
129 promastigote forms (42) suggesting a promastigote-specific function for PKA activity.
130 Here we present a systematic analysis of three PKAC and two PKAR isoforms of *L. mexicana*,
131 using CRISPR-Cas9 gene deletions and microscopy to discover how gene loss affects flagellar
132 beat dynamics. Localisation of fluorescently tagged proteins showed distinct subcellular
133 localisation patterns and dependencies, from which we infer pairing preferences for
134 *Lmx*PKAC1 and *Lmx*PKAC2 with *Lmx*PKAR1 in the flagellum, and *Lmx*PKAC3 with
135 *Lmx*PKAR3 along the cell cortex. Targeted gene deletion of subunits individually and in
136 combination showed that none are essential for promastigote growth. Assessment of swimming
137 speed, and measurement of flagellar waveform parameters showed that disruption of
138 *Lmx*PKAC or *Lmx*PKAR subunits affected motility and we show that *Lmx*PKAC1 is essential
139 for the generation of a symmetrical tip-to base flagellar beat.

140 **Results**

141 ***Leishmania spp. have three PKAC and two PKAR subunits.***

142 BLAST searches with the three PKAC and the single PKAR sequences from *Trypanosoma*
143 *brucei* (38) identified syntenic *Leishmania mexicana* orthologues for all four genes (Table 1)
144 (48). Analysis of the *L. mexicana* PKAC sequences confirmed overall conservation of the
145 trypanosomatid PKAC repertoire: The highly similar *Lmx*PKAC1 and *Lmx*PKAC2 are located
146 on chromosome 34, not in a tandem array but separated by four other genes. This locus is
147 syntenic with the locus of *T. brucei* and *T. cruzi* PKAC1 and PKAC2, but the designation of
148 these PKACs as -1 or -2, respectively, varies between species (Table 1, Supplementary Figure
149 1A). *Lmx*PKAC1 and *Lmx*PKAC2, but not *Lmx*PKAC3, have variable N-terminal extensions
150 which harbour a predicted disordered domain (Supplementary Figure 2A, B) and both the active
151 sites and peptide binding sites within all *Leishmania* PKAC1 and PKAC2 are identical
152 (Supplementary Figure 2C, D). Catalytic activity of eukaryotic PKAC have been shown to be
153 modulated by phosphorylation of several residues, such as threonine-197 in the activation loop
154 which is particularly involved in biological activity (49,50), and is conserved across
155 trypanosomatid PKAC (Supplementary Figure 2E). At the C-terminus, trypanosomatid PKAC1
156 and PKAC3 have a conserved FXXF sequence, where mutating either phenylalanine was
157 shown to diminish catalytic activity (51,52). *Lmx*PKAC2 lacks the first of these phenylalanines

158 (Supplementary Figure 2F). All trypanosomatid PKAC3, including *Lmx*PKAC3, have an 8
159 amino acid C-terminal extension of unknown function (46) (Supplementary Figure 2F).
160 Several reports have highlighted the existence of a second PKAR-like protein within the
161 trypanosomatids (53,54), which was recently given the name PKAR3 in *L. donovani* (55); for
162 consistency, we adopt this terminology here. *L. mexicana* has a syntenic orthologue of PKAR3
163 (Table 1) (Supplementary Figure 1D). All trypanosomatid PKAR3s share a similar protein
164 architecture as canonical PKARs (Figure 1A), with two CNBDs towards the C-terminus,
165 preceded by a so-called autoinhibitory domain (AI) sequence that mimics the phosphorylation
166 targets of PKAC and functions to inhibit the catalytic kinase subunits. This short sequence is
167 typically RRXA(G) in Type I PKARs (PKAR-I) and RRXS(T) in Type II PKARs (PKAR-II)
168 (Figure 1B). In Type I PKARs the alanine (A) or Glycine (G) replaces the phosphorylatable
169 serine (S) or threonine (T) residues found in target downstream substrate sites (56,57).
170 Trypanosomatid PKAR1 sequences all have an RRXT sequence that aligns with the
171 autophosphorylatable RRXS motif in human PKAR-II. The *Leishmania* PKAR3 sequences
172 share the RGAIS motif of the canonical mammalian RRRRGAISAE sequence of the PKAR-
173 Iα AI, but notably are missing the first arginine residue of the Type I PKAR motif RRXA
174 (Figure 1B).
175 Deviations from the canonical PKAR architecture are found at the N-termini (Figure 1A):
176 trypanosomatid PKAR1 proteins lack the dimerization/docking domain (DD) that holds
177 canonical eukaryotic PKA heterotetramer together and anchors it to the amphipathic helix
178 region of an A-kinase anchoring protein (AKAP) (58). Instead, they contain a predicted leucine
179 rich repeat (LRR; IPR032675). PKAR3 sequences, lack a recognisable DD domain or an LRR
180 and instead, there is a short coil domain predicted near the N-terminus of all examined PKAR3
181 sequences. This suggests that the family of divergent kinetoplastid PKAR have evolved
182 subcellular anchoring mechanisms distinct from AKAP.

183 ***The cyclic nucleotide binding domains of Leishmania PKAR subunits deviate from the***
184 ***canonical cAMP binding domain of mammalian PKAR.***

185 Structural studies showed that in all trypanosomatid PKAR1s, there are substitutions to key
186 residues in the phosphate binding cassette (PBC) that impede docking of the cAMP molecule
187 (38): a conserved alanine (A) is replaced by a negatively charged glutamate (E), which is
188 predicted to clash with the phosphate group on the cAMP molecule, and the arginine (R) residue
189 required to dock the exocyclic phosphate has been switched to polar uncharged (R/TN) or
190 aliphatic (R/AV) residues. These changes have been linked to the loss of cAMP activation in *T.*

191 *cruzi* and *T. brucei* PKAR1s, and they are conserved in *Leishmania* PKAR1 sequences (38)
192 (Figure 1C). These findings prompted us to examine in detail the nucleotide binding sites of the
193 PKAR3 subunits. Key residue switches are evident in the parasite PKAR3 CNBDs but with
194 some notable deviations from the PKAR1 patterns (Figure 1C). The first alanine (A) in CNBD-
195 A has been switched to a glycine (G), which depending on pH of the environment, can exist as
196 net positive, neutral or negative from low to high pH respectively. Thus, it is hard to predict if
197 this residue would clash with cAMP docking in the same manner as the glutamate in PKAR1,
198 defined by (38). The alanine on CNBD-B of PKAR3 has been substituted for a glutamate,
199 identical to PKAR1 sequences, and the arginine residues have also been substituted in PKAR3
200 CNBD-A and CNBD-B with polar uncharged (R/STN) or hydrophobic side chains (R/A). Most
201 surprisingly is that the conserved initial glutamate within the PBC (G**E**LAL), which forms a
202 hydrogen bond with the 2'-OH moiety on the ribose sugar of cAMP, has been switched to an
203 aspartic acid (D) in PKAR3 CNBD-A and aspartic acid or glutamine (D/Q) in all PKAR3
204 CNBD-B asides from *Lmx*PKAR3. These changes suggest that PKAR3, like PKAR1, has
205 diverged from cAMP binding, but raise the question whether the same or different ligands bind
206 to these sites.
207 All parasite sequences for PKAR1 and PKAR3 have an extended C-terminus end relative to the
208 canonical mammalian PKAR reference sequence (Figure 1A). Two tyrosine (Y) and two valine
209 (V) residues were implicated in forming a parasite specific hydrophobic pocket documented in
210 *Tc*PKAR1 (denoted by orange asterisks in Figure 1C and D), interactions with which were
211 shown to increase the binding affinity and activation potential of certain nucleoside analogues
212 (38). All parasite PKAR1 sequences, contain at least two of these YV residues. Contrastingly,
213 in PKAR3 sequences, *Leishmania* only have one Y and one V, where *Tc*PKAR3 has three of
214 the four hydrophobic residues. Taken together these data indicate that a divergent PKAR1 is
215 conserved in all trypanosomatids, and an additional PKAR3 is found in *Leishmania* spp. and *T.*
216 *cruzi*, with an unknown ligand specificity, that shares in its CNBD sequences some of the
217 divergent features of PKAR1.

218 ***L. mexicana PKACs and PKARs show distinct localisation patterns in the flagellar axoneme***
219 ***and cell body cortex.***

220 To establish the subcellular localisation of the different PKAC and PKAR subunits in *L.*
221 *mexicana* in different cell- and life cycle stages, we inserted fluorescent protein fusion tags
222 (mNeonGreen, mNG) at the endogenous gene loci, producing mutants expressing either N- or
223 C-terminal fusion products for each PKA subunit.

224 mNG::PKAC1 localised to the flagellar axoneme in non-dividing cells (1 kinetoplast, 1 nucleus,
225 1 flagellum (1K1N1F) (59), a signal that remained strong in 0.1% NP-40 detergent-extracted
226 cytoskeletons (Figure 2A). Through the cell division cycle, the signal abundance diminished in
227 the axoneme and increased within the nucleus (Supplementary Figure 3A), corroborating the
228 nuclear localisation that was reported for this protein in a *L. mexicana* kinase localisation screen
229 (60). Strikingly, within the nucleus, the *Lmx*PKAC1 signal intensity was consistently strongest
230 in areas of low Hoechst staining (Supplementary Figure 3A'), suggesting association with the
231 nucleolus specifically. The *Lmx*PKAC1 signal re-appeared in the axonemes of both the old and
232 the newly growing flagellum at cytokinesis. In axenic amastigotes, the mNG::PKAC1 signal
233 appeared greatly diminished, with weak variable cytoplasmic signal (Figure 2A). Fusion of
234 mNG to PKAC1 at the C-terminus disrupted the localisation to the axoneme (Supplementary
235 Figure 4A), as previously reported (41).
236 The mNG::PKAC2 signal was partitioned between the flagellum, the cell body and cortex
237 throughout in the promastigote, with variations in relative intensity in the different
238 compartments at different cell cycle stages (Figure 2B and Supplementary Figure 3B). Notably,
239 in early promastigote division (2F1N1K), the *Lmx*PKAC2 signal appeared enriched in the new
240 growing flagellum and a strong cell cortex signal was seen during mitosis (Supplementary
241 Figure 3B). The *Lmx*PKAC2 axonemal signal was lost from detergent-extracted cytoskeletons,
242 and only a weak variable cytoplasmic signal was seen in axenic amastigotes (Figure 2B). Fusion
243 of mNG to the C-terminus hindered protein localisation to the axoneme (Supplementary Figure
244 4B).
245 The mNG::PKAC3 signal was associated with the cell body cortex in non-dividing cells, with
246 a signal that was strongest at the central region of the cell body and tapering off towards the
247 posterior pole (Figure 2C). In 95% of non-dividing cells, a distinctive 'edge effect' was evident
248 (Figures 2C and 3A) (61). A faint detergent-soluble signal was also present in the flagellum,
249 with an intensity gradient decreasing towards the distal flagellum (Figure 3F). In dividing
250 promastigotes, the *Lmx*PKAC3 signal appeared more uniform across the cell body cortex, with
251 an accumulation at the anterior end of the developing cleavage furrow and a reduced flagellar
252 signal (Supplementary Figure 3C). The promastigote cortex signal disappeared in detergent
253 treated cells and showed a weak variable cytoplasmic signal in the cell body of axenic
254 amastigotes (Figure 2C).
255 PKAR1::mNG showed a strong flagellar axoneme signal in promastigote forms, with a fainter
256 diffuse cell body signal throughout all stages of promastigote cell division (Figure 2D, F). Upon
257 membrane extraction with 0.1% NP-40, the fluorescent signal remained in the axonemal

258 cytoskeleton. Fusion of mNG to the N-terminus of PKAR1 resulted in a reticulated cell body
259 signal, suggesting that blocking the LRR domain may affects protein targeting (Supplementary
260 Figure 4D). After induction of axenic amastigote differentiation for three days, a strong
261 PKAR1::mNG signal was observed in the cytoplasm of axenic amastigotes (Figure 2D).
262 Both N- and C-terminally tagged *Lmx*PKAR3 localised exclusively to the cell body cortex in
263 live promastigotes (Figure 2E and Supplementary Figure 4E). This signal was detergent
264 extractable (Figure 2E), suggesting *Lmx*PKAR3 is anchored weakly to the cortical cytoskeleton,
265 or is associated with the plasma membrane. In axenic amastigotes, the *Lmx*PKAR3 signal
266 persisted at the cell body cortex (Figure 2E). Closer examination of the different cell cycle
267 stages showed that in non-dividing (1F1N1K), and early dividing (2F1N1K) promastigote cells,
268 the cortical *Lmx*PKAR3 signal was most intense in the cell body mid-zone and tapered off
269 towards the posterior pole (Figure 2G, quantified in Figure 3F). In late division (2F2K1N /
270 2F2K2N), the *Lmx*PKAR3 signal intensity became more uniform along the cortex, occasionally
271 appearing enriched at the posterior pole (Figure 2G).
272 Overall, these data show that PKA concentrations in *L. mexicana* vary across sub-cellular space
273 and over time, with two dominant PKA structures being the promastigote flagellum (dominated
274 by *Lmx*PKAC1, -C2 and -R1) and the cell cortex of promastigotes and amastigotes
275 (*Lmx*PKAC3 and -R3). Within these dominant structures, there were cell-cycle stage dependent
276 changes in signal intensity and also a transient shift of the *Lmx*PKAC1 signal in dividing cells
277 into the nucleus and away from the flagellum.

278 ***Localisation dependencies.***

279 Given the striking similarities in the localisation of *Lmx*PKAC3 and *Lmx*PKAR3 at the cell
280 cortex (Figure 2C, 2E), and the strong axonemal localisation of *Lmx*PKAC1 and *Lmx*PKAR1,
281 the question arose whether there were specific PKAC-PKAR pairings in different cellular
282 compartments. To test whether the localisation of any PKAC subunit was dependent on the
283 expression of specific PKARs, we deleted the *Lmx*PKAR1 or *Lmx*PKAR3 genes in cells
284 expressing tagged *Lmx*PKAC1, *Lmx*PKAC2 or *Lmx*PKAC3. Following deletion of *Lmx*PKAR1,
285 promastigotes no longer showed the strong axonemal *Lmx*PKAC1 signal that was seen in the
286 parental cell line (Figure 3B). Similarly, the flagellar signal from *Lmx*PKAC2 was also
287 diminished upon deletion of *Lmx*PKAR1 (Figure 3C). By contrast, deletion of *Lmx*PKAR1 had
288 no visible effect on *Lmx*PKAC3 localisation at the cell cortex (Figure 3D). We then tested
289 whether loss of *Lmx*PKAR3 would affect *Lmx*PKAC3 localisation and found that the distinct
290 cortical signal of *Lmx*PKAC3 became diminished and the signal appeared to become more

291 widely distributed throughout the cell body (Figure 3E). This change in signal distribution was
292 quantified over a cross-section of the cell body, between the kinetoplast and the nucleus. This
293 showed a complete loss of the edge effect for *Lmx*PKAC3 signal after *Lmx*PKAR3 was deleted
294 (Figure 3A, iii). Secondly, the change in signal distribution along the axis of the cell was
295 assessed using a 6-point quantitation technique for fluorescent intensity (Figure 3F). In a
296 parental background, the signal profile of *Lmx*PKAC3 was at its lowest at the distal flagellum,
297 gradually increasing in intensity towards the pocket region (Figure 3F). Following deletion of
298 *Lmx*PKAR3 the *Lmx*PKAC3 signal increased in the flagellum and the cell body gradient was
299 decreased (Figure 3F). Taken together, these data suggest that in non-dividing promastigotes,
300 *Lmx*PKAR1 anchors *Lmx*PKAC1 and *Lmx*PKAC2 in the flagellar axoneme, whilst *Lmx*PKAR3
301 docks *Lmx*PKAC3 at the cell body cortex.
302 Finally, as several publications reported an association of PKA with the radial spokes of the
303 flagellar axoneme, e.g. via the AKAP domain of RSP3 in *Chlamydomonas* (62–64), we asked
304 whether the *Lmx*PKAR1 was associated with the radial spokes of the *Leishmania* axoneme. We
305 deleted radial spoke proteins of the head (RSP9), and stalk (RSP3 and RSP11) (65) in the
306 PKAR1::mNG expressing cell line to see if the axonemal signal disappeared. A PKAR1::mNG
307 signal was still observed in the axoneme of the examined RSP knockouts, including the short
308 axonemes that are characteristic of RSP3 deletion mutants (Supplementary Figure 4F-I). These
309 data suggest that flagellar PKA localisation does not depend on the integrity of the radial spokes
310 in *Leishmania*, consistent both with the lack of a DD domain in *Lmx*PKARs and the recognition
311 that whilst the RSP3 AKAP domain is homologous to PKA-binding AKAP sequences, its
312 function in the axoneme is docking of non-PKA RII domain proteins (66,67).

313 ***Toyocamycin exposure dissociates PKAC1 signal from the axonemal cytoskeleton.***

314 To determine whether *Lmx*PKAR1 could be pharmacologically activated by toyocamycin as
315 was shown in *Trypanosoma* spp. (38), cytoskeletons from mNG::PKAC1 expressing cells were
316 incubated with cAMP or toyocamycin prior to imaging and quantification of axonemal
317 fluorescence (Figure 4). In addition to these, we tested the effect of inosine, considering that it
318 is similar in structure to toyocamycin (which derives from *Streptomyces* (68)) but perhaps more
319 biologically relevant since it is present endogenously as part of purine metabolism pathways
320 (69).
321 The axonemal mNG::PKAC1 signal remained strong after treatment with cAMP, up to 100 μM
322 (Figure 4B), however quantification revealed a small but significant decrease in fluorescent
323 signal relative to untreated cytoskeleton controls (Figure 4E). By contrast, the mNG::PKAC1

324 signal was diminished after treatment with 1 μM toyocamycin and completely lost in most cells
325 upon addition of 100 μM toyocamycin (Figure 4C, 4E). Loss of the mNG::PKAC1 signal was
326 also observed upon treatment with 1 μM and 100 μM inosine, with a greater reduction of
327 fluorescence intensity at each concentration, compared to toyocamycin (Figure 4D, 4E).

328 ***LmxPKAC1 plays an important role in flagellar motility.***

329 We previously showed that partial deletion of *Lmx*PKAC1 (*ΔLmxM.34.4010*) reduced
330 promastigote swimming speed (41). Here we employed the same CRISPR-Cas9 knockout
331 strategy to generate the full knockout cell lines *ΔLmxPKAC1*, *ΔLmxPKAC2* and *ΔLmxPKAC3*
332 as well as *ΔLmxPKAR1* and *ΔLmxPKAR3* (Supplementary Figure 5) to measure precisely how
333 the loss of each of these proteins affected flagellar motility. The null mutants were all viable as
334 promastigotes, with comparable *in vitro* growth rates as the parental cell line (Supplementary
335 Figure 6). The swimming behaviour of null mutant populations was measured with the same
336 method used in (41) and the results (Figure 5A) confirmed that promastigotes lacking
337 *Lmx*PKAC1 swam statistically slower (average 4.9 μm/s ± 0.035 standard deviation, unpaired
338 t-test assuming equal variance ($p < 3.5 \times 10^{-14}$) than the parental cell line (7.4 μm/s ± 0.917).
339 See Supplementary Table 1 for raw speed and directionality measurements and the respective
340 p-values. A reduced mean population swimming speed was also observed for *ΔLmxPKAC3* and
341 *ΔLmxPKAR1* (5.7 μm/s ± 0.032 and 5.4 μm/s ± 0.273, respectively); deletion of *LmxPKAR3*
342 had the opposite effect and resulted in an elevated swimming speed (8.4 μm/s ± 0.775). By
343 contrast, deletion of axonemal *Lmx*PKAC2 did not significantly alter parasite swimming speed
344 (average 6.4μm/s ± 0.650, unpaired t-test, $p = 0.093$) (Figure 5A). To test what the combined
345 effect was of deleting *Lmx*PKAC1 and either *Lmx*PKAR3 or *Lmx*PKAC2 in the same cells, the
346 respective double null mutants were generated (Supplementary Figure 5B). These showed the
347 same reduced swimming speed as the *ΔLmxPKAC1* population (Figure 5A), indicating that loss
348 of *Lmx*PKAC1 was the dominant cause of the observed slow motility phenotype, which could
349 not be rescued or further compounded by secondary gene deletion of *Lmx*PKAR3 or
350 *Lmx*PKAC2.

351 ***LmxPKAC1 is required for the generation of symmetric flagellar waves.***

352 Since swimming speed measurements report the average for a whole population, we next used
353 high speed video microscopy, alongside semi-automated tracing scripts (70,71), to further
354 dissect how deficiency of each PKA subunit was affecting the flagellar beat of individual cells.

355 First we used population overview waveform analysis (POWA), described in (72), capturing
356 0.5 seconds of high speed (200 Hz) low magnification (×20) videos to assess the relative
357 proportions of the different waveforms that *L. mexicana* are known to generate: the tip-to-base
358 symmetric flagellar waveform, the base-to-tip asymmetrical ciliary waveform (Figure 5B), or,
359 an undefined aperiodic movement referred to as uncoordinated.
360 *ΔLmxPKAC3* and *ΔLmxPKAR3* showed similar proportions of cells performing flagellar beats
361 as the parental cells (~75%), however all PKA null mutants appeared to display fewer instances
362 of ciliary beats and a greater proportion of cells (> 25%) moving in an uncoordinated manner
363 (Figure 5C). *ΔLmxPKAC2* and *ΔLmxPKAR1* both displayed a lesser proportion of cells
364 propagating the flagellar wave (< 65%). Strikingly, *ΔLmxPKAC1* cells were completely unable
365 to propagate the typical tip-to-base symmetrical flagellar waveform and instead showed
366 completely uncoordinated flagellum movements (Figure 5C). This observation demonstrates
367 that *Lmx*PKAC is essential for producing a symmetric and rhythmic flagellar movement.
368
369 ***All PKAC subunits contribute in different ways to beat amplitude and frequency.***
370 In order to dissect how the loss or dysregulation of PKA contributes to the overall waveform,
371 we used cell tracing and Fourier analysis to extract the dominant beat frequency, amplitude and
372 waves per flagellum comprising the tip-to-base flagellar waves (70,71). *L. mexicana* flagellar
373 waves usually beat 20-35 times per second (Hz) with a maximum shear angle amplitude
374 (relative to the flagellum base) between 40 to60 degrees along the flagellum (71,73). This was
375 confirmed here for the parental control cell line (Figure 6, Table 2 with p-values listed in
376 Supplementary Table 2). *ΔLmxPKAC1* were never observed propagating a rhythmic symmetric
377 flagellar wave (Figure 6A). Our best effort to fit a dominant frequency of attempted tip-to-base
378 movements showed a greatly diminished frequency (< 10 Hz), with shear angle amplitudes not
379 exceeding 30 degrees (Figure 6B), indicating that *Lmx*PKAC1 is required for the generation of
380 a normal flagellar beat. The flagellar length and wavelength are coupled in *Leishmania* spp.,
381 leading to tendency of ~1 wavelength per flagellum (74). We saw here that these parameters
382 showed a positive correlation in all PKA knockout cell lines (Spearman's rank correlation
383 coefficient, except *ΔLmxPKAC1* cells (Supplementary Figure 7). Flagellar waves from
384 *ΔLmxPKAC2* displayed a slight but significantly diminished beat amplitude (Figure 6C). We
385 also observed that *ΔLmxPKAC3* had significantly diminished beat frequencies (averaging 22
386 Hz), but otherwise displayed normal beat amplitudes (Figure 6D). *ΔLmxPKAR1* retained
387 comparable flagellar wave parameters relative to parental control cells (Figure 6E). Lastly,

388 although *ΔLmxPKAR3* and *ΔLmxPKAC2* mutants showed a comparable average beat frequency
389 for flagellar waves to control populations, the measured values appear to show a bimodal
390 distribution, with a sub-population with low beat frequency (~15 Hz) and one with an
391 abnormally high beat frequency (> 40Hz) (Figure 6C, 6F). The normal average population
392 speed for *ΔLmxPKAC2* and elevated population swimming speed for *ΔLmxPKAR3* (Figure 5A)
393 could have arisen from the averaging of these extreme values. More cells would need to be
394 captured, and perhaps observed over longer time periods, to ascertain the true relative
395 proportions of these phenotypes in the population and assess whether individual flagella can
396 switch between abnormally low and high frequencies.
397 Taken together, these measurements show that removal of different PKA subunits perturbed
398 the flagellar beat of *L. mexicana* in specific ways. Removal of the catalytic subunit PKAC1,
399 which is normally docked to the flagellar cytoskeleton through association with PKAR1, had
400 the biggest effect; without PKAC1 the flagellar waveforms lost their symmetry and this
401 uncoordinated beating reduced the speed at which the cells swam.

402 **Discussion**

403 Protein kinase A is one of the most studied eukaryotic signal transducers, which is highly
404 conserved throughout the eukaryotes (excluding plants (75)). PKA signalling fine-tunes a
405 multitude of cellular processes and our interest centred on the role of PKA in the modulation
406 of flagellar beating. In kinetoplastids, converging evidence from proteomics and
407 transcriptomics datasets and mutant phenotypes suggested PKA may also have a role in
408 flagellar motility. Here, we used a genetic approach combined with fluorescence- and video-
409 microscopy, to dissect the localisations and paring preferences of the three *L. mexicana* PKAC
410 and two PKAR proteins and studied how gene deletions impacted cell swimming and
411 generation of flagellar waveforms. Our results corroborate recent reports of PKAC/R pairings
412 in *Leishmania* (55) and extend previous analyses on PKA function by providing multiple lines
413 of evidence for a vital function for *Lmx*PKAC1 in flagellar beat regulation. We found that there
414 are two regions of PKA concentration in promastigote forms: *Lmx*PKAC1, *Lmx*PKAC2 and
415 *Lmx*PKAR1 showed enrichment in the flagellum, while a strong cell body cortex signal was
416 detected for *Lmx*PKAC3 and *Lmx*PKAR3. These localisations were neither exclusive nor static
417 and examination of cells at different stages in the division cycle indicated dynamic
418 relocalisation of all three *Lmx*PKAC subunits and of *Lmx*PKAR3; only *Lmx*PKAR1 maintained
419 its dominant flagellar signal in all examined cells, and it was embedded within the axoneme

420 sufficiently strongly to withstand detergent extraction. Upon deletion of *Lmx*PKAR1, the
421 flagellar signal of *Lmx*PKAC1 was greatly diminished and we conclude that *Lmx*PKAR1 is the
422 anchor that holds *Lmx*PKAC1 in the axoneme. Based on all available knowledge of PKA
423 activation mechanisms, our assumption is that while bound to *Lmx*PKAR, *Lmx*PKAC is
424 inactive.
425 Analysis of the motility phenotypes of gene deletion mutants showed that *Lmx*PKAC1 was
426 essential for propagation of symmetric flagellar waveforms used for forward motility. All of
427 the PKA mutant cell lines were viable and remained motile (including the double deletion of
428 *Lmx*PKAC1 and *Lmx*PKAC2), but measurement of mean population swimming speeds showed
429 differences compared to the parental control line for all null mutants except the *ΔLmxPKAC2*.
430 *ΔLmxPKAC1* showed the greatest reduction in swimming speed and this mutant was unique in
431 its complete inability to generate any symmetric tip-to-base flagellar waves, instead beating its
432 flagella in an uncoordinated manner characterised by a lack of rhythm, symmetry and a very
433 low dominant beat frequency and reduced amplitude compared to normal flagellar waveforms
434 of promastigotes. These data suggest *Lmx*PKAC1 is required within the axoneme to maintain
435 the appropriate spatio-temporal activation of axonemal dyneins, most likely as a component of
436 a signal transduction cascade that leads to the phosphorylation of either core axonemal proteins
437 that regulate dyneins, or of dynein subunits directly. The ODAs, which are important for beat
438 frequency (29), are thought to be a key target of cAMP-dependent protein kinase (PKA)
439 (models, reviewed in (17,36)). Outer dynein light chain proteins from the ciliates *Paramecium*
440 *tetraurelia* (p29 (76)) and *Tetrahymena* (p34 (28)) were shown to be phosphorylated upon
441 treatment with cAMP and RNAi knockdown of *P. tetraurelia* outer dynein light chain 1
442 (ODLC1) resulted in loss of phosphorylated p29 and rendered cilia unresponsive to cAMP (30).
443 The cAMP-independent PKA may be targeting the conserved homologous structures in
444 kinetoplastids. Phosphoproteomic data gained from exposing *T. brucei* parasites to a synthetic
445 PKA activator, 7-CN-7-C-ino, identified phosphopeptides for several proteins with known
446 functions in normal motility including several dynein intermediate chains (IC138), distal
447 docking complex 2 (dDC2) and nexin dynein regulatory complex-2 (38). Comparisons of
448 phosphorylation patterns in axonemes of *L. mexicana* PKA mutants and wild type controls
449 could further corroborate these strong candidates for *Lmx*PKAC1 phosphorylation substrates.
450 In addition to confirming the phosphorylation substrates, further dissection of the mechanism
451 will benefit from studies examining how the putative substrates affect flagellar waveform
452 modulation and how that would be altered if the phosphorylated residue were mutated to a
453 neutral or to a charged residue. Another fruitful avenue to defining the *Lmx*PKAC1 signalling

454 pathway might be pinpointing where in the axoneme the *Lmx*PKAR1/C1 complex is docked, a
455 question that will require molecule-level resolution obtained from techniques such as cryo-
456 electron microscopy. Cells lacking *Lmx*PKAR1 also swam significantly slower, and this mutant
457 lost most of its flagellar *Lmx*PKAC1 signal. This is consistent with a model where axonemal
458 *Lmx*PKAR1 binds and concentrates PKAC1 along the flagellum, placing it in proximity to
459 axonemal proteins which are phosphorylated upon receipt of an activating signal.
460 Of course, it is not unusual for kinases to have pleotropic function and moreover, localisation
461 of proteins does not necessarily indicate function within that domain. Likewise with the
462 observed dual localisation of *Lmx*PKAC1, its localisation in the axoneme in non-dividing cells
463 could be, in part, a sequestration away from other targets within the cell body or nucleolus,
464 which may be involved in replication events. However, while the mutant analysis revealed a
465 clear motility phenotype upon loss of *Lmx*PKAC1, cell growth remained unaffected, arguing
466 against a key role in the regulation of cell division events. Alternatively, during division, where
467 forward swimming may need to be dampened, *Lmx*PKAC1 may be partitioned to the nucleus
468 until returning to the new and old flagella axonemes. Experiments involving pulse-chase
469 labelling of proteins would be required to assess the relationship between the different
470 *Lmx*PKAC1 populations fractions over the course of the cell cycle. In any case, the activation
471 status of *Lmx*PKAC1 in the nucleus remains an open question. *Lmx*PKAR1 was never observed
472 alongside its catalytic subunit in the nucleolus during division and this spatial uncoupling would
473 presumably populate the nucleolus with active *Lmx*PKAC or, if sequestration was the purpose,
474 require an alternative regulatory mechanism for *Lmx*PKAC inactivation.
475 *Lmx*PKAC1 and *Lmx*PKAC2 share 86% sequence identity and localisation data suggest
476 *Lmx*PKAR1 is required for both their enrichment in the flagellum. Unlike *Lmx*PKAC1,
477 however, *Lmx*PKAC2 was solubilised by treatment with 0.1% NP-40 while *Lmx*PKAC1
478 remained in the flagellar cytoskeletons. Furthermore, loss of *Lmx*PKAC2 had only a small
479 effect on flagellar beat dynamics when observed at the level of populations: *ΔLmxPKAC2*
480 displayed comparable population swimming speeds to parental controls, with only a small
481 increase in the proportion of cells exhibiting uncoordinated flagellar waveforms (Figure 5C).
482 The observation that the frequencies of flagellar waveforms of individual cells segregated into
483 two groups, low frequency or high frequency, suggests that *Lmx*PKAC2 may have a role in
484 maintaining a constant beat frequency. The POWA measurements represent snapshot
485 observations of flagella over a short time period. To study this further, it would be informative
486 to observe individual cells for a longer time to determine if periods of low frequency waves
487 alternate with high frequency waves in single flagella.

488 *Lmx*PKAC3 had a clearly distinct localisation, concentrated at the cell cortex, similar to
489 *Lmx*PKAR3. The peripheral enrichment was lost upon deletion of *Lmx*PKAR3, suggestive of a
490 *Lmx*PKAC3/R3 complex. A faint flagellar signal was also observed for *Lmx*PKAC3, which was
491 increased in the *ΔLmxPKAR3* deletion mutant. Interestingly, the motility phenotype of gene
492 deletion mutants correlated with changes of *Lmx*PKAC3 abundance in the flagellum: the
493 *ΔLmxPKAC3* population swam more slowly and *ΔLmxPKAR3* swam faster than parental
494 controls. The slower swimming speed for *ΔLmxPKAC3* was likely the combined effect of the
495 increased proportion of cells showing uncoordinated beating and the slight decrease in the beat
496 frequency of flagellar waves. Additionally, there was a small reduction in average flagellum
497 length (Figure 5D). Interestingly, loss of *Lmx*PKAR3, which led to a re-distribution of
498 *Lmx*PKAC3 away from the cell cortex, resulted in more cells propagating flagellar beats
499 exceeding 40Hz and increased mean population swimming speed. It remains an open question
500 whether *Lmx*PKAC3 has bona-fide phosphorylation targets within the flagellum, or whether
501 the increased amount of soluble catalytic subunit in the *Lmx*PKAR3 deletion mutant causes off-
502 target phosphorylation events in the axoneme that affect motility, secondary to its main role
503 elsewhere. A recent report linked *Lmx*PKAR3 and *Lmx*PKAC3 to processes involved in cell
504 morphology in *L. donovani* (55). This may explain the shortened flagella in our *ΔLmxPKAC3*
505 cells but we did not observe any morphological changes in *ΔLmxPKAR3*. Moreover, all of our
506 *L. mexicana* PKA KO lines here showed normal cell growth and maintained the same mean
507 cell pseudo-diameter as the parental controls (Supplementary Figure 6B).
508 Owing to the high conservation of PKA, it has long been presumed that its activation
509 mechanism through cAMP was equally as conserved, until the recent discovery that
510 trypanosome PKA is insensitive to cAMP and instead activated by a different ligand (38).
511 Multiple lines of evidence indicate that this alternative PKA activation pathway also operates
512 in *L. mexicana*. First, the sequences of the *Lmx*PKAR1 and *Lmx*PKAR3 phosphate binding
513 cassettes showed the characteristic residue switches that were shown in Trypanosoma to
514 prevent cAMP binding. However, while *Lmx*PKAR1 and *Lmx*PKAR3 both have some of the
515 distinctive features of Trypanosoma PKAR1, the loss of a typically invariable glutamate in
516 most PKAR3 PBCs raises the question whether this subunit could bind a different ligand to the
517 kinetoplastid PKAR1. As this glutamate within the PBC is known to hydrogen bond with the
518 ribose hydroxyl group in cyclic nucleotide molecules (77), we could speculate that the unknown
519 ligand is not centred around a ribose sugar. Second, we showed that treatment of cytoskeletons
520 with cAMP had very little effect on the axonemal localisation of mNG: *Lmx*PKAC1 while

521 exposure to toyocamycin and inosine reduced the axonemal *Lmx*PKAC1 signal substantially
522 (Figure 4). This fits the model of the *T. brucei* PKAR1/C2 complex, where toyocamycin
523 binding to PKAR resulted in the release of the catalytic subunit and subsequent substrate
524 phosphorylation (38). These data together are consistent with a scenario whereby ligand binding
525 causes a conformational change in axonemal *Lmx*PKAR1 which releases *Lmx*PKAC1 into the
526 soluble fraction, and confirms published findings that the ligand for divergent parasite PKA is
527 likely not a cyclic nucleotide, but instead a nucleoside analogue either endogenously produced
528 or exogenously sourced. As inosine is an intermediate compound of the purine metabolism
529 pathway (69), it is tempting to speculate that the potential endogenous ligand for divergent
530 kinetoplastid signalling pathway is a derivative of this pathway.
531 Although the role of cAMP-responsive PKA in flagellar signalling has been established (78,79),
532 these data indicate that in kinetoplastids, the divergent (non-cAMP-responsive) PKA maintains
533 a function in motility regulation and suggests that the physiological ligand(s) of kinetoplastid
534 PKARs modulate the swimming behaviour of *Leishmania* promastigotes.
535

536 **Methods**

537 ***Cell culture***

538 A *Leishmania mexicana* (WHO strain MNYC/BZ/62/M379) cell line expressing Cas9 and T7
539 RNA polymerase (80) was used as a parental cell line throughout this project unless stated
540 otherwise. Promastigote form cells were cultured exactly as described in (80). In brief, cells
541 were incubated at 28°C and maintained in M199 (Life Technologies) medium supplemented
542 with 2.2 g/L sodium bicarbonate between $1x10^5$ and $2x10^7$ cells/ml with regular sub-culturing.

543 ***Endogenous fluorescent tagging and gene deletion***

544 Gene knockouts and cell lines expressing endogenously fused fluorescent gene products were
545 essentially created as outlined by Beneke *et al*., (80). An online resource for automated primer
546 design (www.LeishGEdit.net) was used to obtain primer sequences for the replacement of
547 target gene ORFs with drug resistance cassettes (pT plasmids used to create donor products) or
548 insertion of mNeonGreen (pPLOT plasmids used to create donor products) to the endogenous
549 gene locus (80). Promastigote populations transfected with DNA donor and guide constructs
550 were maintained in M199 medium supplemented with relevant selection drugs (either 20 μg/ml

551 puromycin, 5 μg/ml Blasticidin or 40 μg/ml G418) for 3 culture passages before performing a
552 PCR based knockout verification.

553 ***Diagnostic PCR for gene knockout validation.***

554 Primers sequences targeting the open reading frames (ORF) of genes of interest (GOI) were
555 taken from the LeishGEdit primer database (www.LeishGEdit.net) and sourced from
556 ThermoFisher. Due to high sequence similarity, *LmxPKAC1* and *LmxPKAC2* gene deletion
557 verification, primers were manually designed using Primer3 (see Table 3 for primer sequences
558 and corresponding PCR amplicon sizes). To test for presence or absence of a GOI, the relevant
559 forward and reverse (F/R) primers (Table 3, Columns 3-4) were used to amplify a fragment of
560 the ORF from genomic DNA from the parental cell line (positive control) and genomic DNA
561 from the knockout mutant. A PCR reaction targeting a "housekeeping" gene, here PF16
562 (LmxM.20.1400), was run in parallel as a technical control. Master mixes for the PCR reactions
563 constituted the FastGene Optima HotStart Ready Mix sourced from Nippon Genetics
564 containing 4 ng/μl of the relevant gDNA and 2.5 μM each of the forward and reverse primers.
565 For all diagnostic PCRs, the following PCR program steps were used. Step 1: First denaturation
566 at 95°C for 3 minutes. Step 2: denaturation at 95°C for 15 seconds. Step 3: 58°C for 15 seconds.
567 Step 4: 72°C for 30 seconds. Step 5: repeat steps 2-4 for 30 cycles. Step 6: 72°C for 1 minute.

568 ***Detergent extraction of cell membranes.***

569 Promastigote cytoskeletons were prepared from 1 – 5 ml (depending on the cell culture density
570 assessed by eye) of mid-log cells. Cells were washed once with PBS and the washed pellet was
571 resuspended in 100 μl (or 1 ml if > 1E7 cells are in the sample) PEME [100 mM Pipes, 2 mM
572 EGTA, 1 mM MgSO4 and 100 nM EDTA] with 0.1% NP-40. Once homogenous and the
573 solution turns clear, the sample was spun at 2ºC at 10,000*g* for 5 minutes. The supernatant was
574 removed and the pellets were washed with PEME and then resuspended in PEME or PBS with
575 10 μg/ml Hoechst 33342. For the experiments assessing the fluorescent *Lmx*PKAC1 signal in
576 cytoskeletons, the treatment substance was added to the PEME used during the final wash step
577 at a 1:1000 ratio from a stock solution at 1000x final concentration (cAMP (Sigma-Aldrich
578 A6885), at 1 and 100 mM in water; toyocamycin (Sigma-Aldrich T3580) at 1 and 100 mM in
579 DMSO; inosine (ThermoFisher Scientific A14459); 1 and 100 mM in water). If the substance
580 was dissolved in DMSO, then the respective amount of DMSO (0.1%) was added to the control
581 cytoskeletons in PEME buffer.

582 ***Light microscopy.***

583 For live cell fluorescence microscopy of promastigote cells, 1 ml of a mid-logarithmic culture
584 (between $1x10^6$ – $1x10^7$ cells/ml) was spun at 800*g* for 5 minutes and the pellet resuspended in
585 100 μl of PBS and [10 μg/ml] Hoechst 33342 (ThermoFischer). A volume of 0.7 μl was spread
586 onto a poly-lysine coated glass slide, bordered (~ 5 x 2 cm rectangle) with a hydrophobic fat
587 pen (Dako). A glass coverslip, thickness 1 or 1.5 was used to cover the slide. Live cell imaging
588 was typically done with a Zeiss Axioimager.Z2 microscope with a Hamamatsu ORCA-Flash4.0
589 camera, x63 oil objective lens with numerical aperture (NA) 1.4, and phase contrast
590 illumination. Fluorescence channel was acquired with between 0.5 and 3 seconds of excitation
591 depending on the brightness of the fluorescent signal.
592 For live cell imaging of axenic amastigotes, 500 μl of mid-log promastigote culture was
593 inoculated into a vented 25 cm^3 flask (total 5 ml volume) containing Schneider's Drosophila
594 medium (Life Technologies) supplemented with 20% heat-inactivated foetal bovine serum
595 (FBS) (Gibco) and adjusted to pH 5.5 with concentrated HCl. Cultures were incubated at 34°C
596 with 5% CO_2 for 72 hours prior to imaging. 1 ml of sample culture was pelleted by
597 centrifugation at 800*g* for 5 minutes, pellet washed with PBS, spun again, then the washed
598 pellet resuspended in 50 μl of PBS plus Hoechst 33342 (final 10 μg/ml). A volume of 20 μl
599 was placed on the poly-lysine coated glass slide and left inside a humid chamber for 10 minutes
600 to settle. Excess liquid was gently removed by pipetting and the cover slide placed on top.

601 ***Population overview waveform analysis (POWA).***

602 For POWA, 1 ml of exponential growth phase promastigote cells ($1x10^6$ – $1x10^7$ cells/ml) was
603 centrifuged for 5 minutes at 800*g*. Between 600 – 900 μl supernatant was removed and the cells
604 resuspended in the remaining 400 – 100 μl of M199 medium, effectively concentrating the cells.
605 1 μl of 1:100 bead mix (Sigma 79633 polystyrene microparticle beads (5 μm size) in M199
606 medium) was added to cell suspension and mixed gently until homogenous. 1 μl of cell sample
607 was added to the centre of a glass microscope slide bordered by a Dako hydrophobic pen (~5
608 cm by 2 cm rectangle). A glass coverslip of 1.0 or 1.5 thickness bordered by a similar Dako
609 hydrophobic pen rectangle was placed gently on top of the sample slide, effectively creating a
610 sealed chamber. Videomicrographs of swimming cells under phase contrast illumination were
611 captured with an Andor Neo 5.5 camera at 200 frames/s for 0.5 seconds, using a x20 NA 0.3
612 objective lens on a Leica Inverted microscope. Manual categorisation of waveforms was
613 performed in ImageJ or Fiji (81,82) for non-dividing cells only. Categories include flagellar

614 wave tip-to-base (continuous and interrupted), ciliary asymmetric wave base-to-tip and
615 uncoordinated which is neither flagellar nor ciliary. Flagellar length was measured from stills
616 obtained from these videomicrographs, using the Fiji freehand line measuring tool.
617

618 ***Waveform parameter analysis.***

619 The capture of videomicrographs for waveform analysis was exactly as above (POWA), with
620 the exception of using a x100 NA 1.4 oil immersion objective and capturing for 5 seconds
621 duration. All videomicrographs were captured within 10 minutes of making sample slides.
622 Obtaining tangent angle kymographs from phase contrast videos was done as previously
623 described (83). In brief, automated cell tracing scripts developed for phase contrast videos
624 (Supplementary File 1A PhaseTrace.ijm) (84) were run in ImageJ. Resulting tangent
625 kymographs were manually cropped to exclude the cell body and to a frame length of either
626 128 (0.64 seconds) or 256 (1.28 seconds). Each datapoint on the plots present a discrete unit of
627 time (as above), where several datapoints (up to three) could derive from one cell. Fast Fourier
628 transform (FFT) and PowerPlotter scripts (Supplementary File 1B, 1C respectively) were run
629 to obtain the Fourier power spectrum, which was aggregated over the length of the flagellum.
630 The dominant beat frequency was obtained by determining the highest frequency peak from the
631 FFT output using a sliding window with a width of 10% of the measurable frequency range.
632 Data obtained from Fourier analysis were compiled in Excel and plotted using GraphPad Prism
633 9. Angular amplitude measurements along each flagellum (computed for the identified
634 dominant frequency from the FFT) were averaged and plotted against the dominant frequency.
635 Waves per flagellum length was calculated in Excel by taking the difference in phase of the
636 identified dominant frequency between the proximal and distal ends of flagella, then dividing
637 the phase difference by 2π.

638 **Acknowledgements**
639 A part of this work was carried out at the Wellcome Centre for Integrative Parasitology (WCIP)
640 at the University of Glasgow and we thank the WCIP for hosting SF as a visiting student. We
641 thank Keith Gull (University of Oxford) for access to laboratory equipment at the Dunn School.

642 **Funding statement**
643 EG was supported by a Royal Society University Research Fellowship (UF160661).

SF was supported by a Royal Society Enhancement Award (RGF\EA\180189) and Studentship funding from the Sir William Dunn School of Pathology, University of Oxford.
RJW was supported by the Sir Henry Dale Fellowship (Nuffield Department of Medicine) [211075/Z/18/Z].
BJW was supported by the Royal Commission for the Exhibition of 1851.
We acknowledge support for this project for EG and SF through the WCIP core Wellcome Centre Award [104111/Z/14/Z] and through the Wellcome Trust grant [104627/Z/14/Z] to Keith Gull; https://wellcome.org).
The funders had no role in study design, data collection and analysis, decision to publish, or preparation of the manuscript.

655 **Table 1.** Accession numbers for all PKAR and PKAC orthologues found encoded in the
656 genomes of *L. mexicana, L. major, L. donovani, T. brucei* and *T. cruzi*. Each row represents
657 genes found in a syntenic locus across kinetoplastid species, as illustrated in Supplementary
658 Figure 1A-D.
659

	***L. mexicana* (Lmx)**	***L. major* (Lmj)**	***L. donovani* (Ld)**		***T. brucei* (Tb)**	***T. cruzi* (Tc)**
PKAR1	LmxM.13.0160	LmjF.13.0160	LdCL_130006600	**PKAR1**	Tb927.11.4610	TcCLB.506227.150
PKAR3	LmxM.33.2820	LmjF.34.2820	LdCL_340034800	**PKAR3**	n/a	TcCLB.510879.50
PKAC1	LmxM.34.4010	LmjF.35.4010	LdCL_350045700	**PKAC2**	Tb927.9.11100	TcCLB.508461.310
PKAC2	LmxM.34.3960	LmjF.35.3960	LdCL_350045200	**PKAC1**	Tb927.9.11030	TcCLB.508461.280
PKAC3	LmxM.18.1080	LmjF.18.1080	LdCL_180016100	**PKAC3**	Tb927.10.13010	TcCLB.509805.10

660
661

662 **Table 2. Flagellar waveform summary.** For each null mutant cell line, the following numbers
663 are shown: Number (n) of timepoints captured by high-speed video microscopy, where each
664 timepoint represents 256 video frames, and n cells captured in total; the total time observed for
665 each mutant dataset in seconds. The mean amplitude (amp) in degrees (deg); mean beat
666 frequency (beats per second, bps; Hz); number of waves per flagellum (w/f); flagellum length
667 in μm and n of cells for which length was measured. Mann-Whitney u test was used to ascertain
668 significance of each dataset against that of the parental control measurements. Significant p-
669 values are indicated as, *** = $p < 0.001$, ** = $p < 0.005$, * = $p < 0.05$. All p-values can be found
670 in Supplementary Figure 7.
671

mutant Δ	n timepoints (n cells)	total time obs (s)	mean Hz (bps)	mean amp (deg)	waves per flagellum (w/f)	F-length (µm) (n cells)
ΔLmxPKAR1	24 (17)	32.6	28	37	0.84	15.5 (57)
ΔLmxPKAR3	15 (10)	20.4	33	39	0.91	15 (88)
ΔLmxPKAC1	25 (17)	34	4***	26***	1.01	14.6 (93)
ΔLmxPKAC2	13 (7)	17.7	32	34*	1.08*	13.9 (97)
ΔLmxPKAC3	25 (15)	34	22***	41	0.79	13*** (143)
parental	35 (21)	48	27	41	0.85	15.2 (75)

672
673
674 **Table 3.** Primer sequences used for PCR based gene deletion verification, including gene target
675 and ID (columns 1-2), forward and reverse primer sequences (columns 3-4) and the expected
676 PCR amplicon length in nucleotides (nt) (column 5).
677

Gene target	Gene ID	Primer sequences: forward / reverse		PCR amplicon length (nt)
LmxPKAC1	LmxM.34.4010	TCATTGGGCCA ACTCAGCAGC	CATTTGGCGTGACAG CCCCCT	91
LmxPKAC2	LmxM.34.3960	TGGAGCCGAAA CCTGAGGTGGC	CCGCGTACACTCGTC CTCCTGG	70
LmxPKAC3	LmxM.18.1080	GCACAAAGGAA CAGGCCAGTAC	ACAGCCGGTTCTTGT CCATGTA	167

LmxPKAR1	LmxM.13.0160	AAACCTTCGACAGCATCCTCGA	GTTCGAGATGGGGTTGTTGCTG	254
LmxPKAR3	LmxM.33.2820	GCGTTGAATCGGGAAAACTCGT	CCATCTCCTGACGTCCAAACCT	121
PF16	LmxM.20.1400	CCAGCACTGTGTCTACCTACCC	TGATGATCTGGATGGACTCGGC	212

678

679

680 **Figure Legends**

681

682 **Figure 1. Alignments of PKAR sequences.**

683 **(A)** Cartoon representation of trypanosomatid PKAR proteins *Ld*PKAR1
684 (LdBPK.13.2.000160), *Lmj*PKAR1 (LmjF.13.0160), *Lmx*PKAR1 (LmxM.13.0160),
685 *Tb*PKAR1 (Tb927.11.4610), *Tc*PKAR1 (TcCLB.506227.150), *Ld*PKAR3
686 (LdBPK.34.2.002680), *Lmj*PKAR3 (LmjF.34.2820), *Lmx*PKAR3 (LmxM.33.2820),
687 *Tc*PKAR3 (TcCLB.510879.50), and Homo sapiens cAMP-dependent protein kinase type I-
688 alpha regulatory subunit PKAR-I**α** (P10644, KAP0_HUMAN) and type II-alpha regulatory
689 subunit PKAR-II**α** (P13861|KAP2_HUMAN). LRR, leucine rich repeat; DD, dimerization
690 docking domain; CNBD, cyclic nucleotide binding domains (PFAM ID: PF00027); AI,
691 autoinhibitory domain sequence (56). **(B)** AI sequence alignment. Bold letters highlight the
692 RRxA and RRxT motifs which form a pseudo-substrate or are autophosphorylated by docked
693 catalytic subunits in mammalian PKA heterotetramers. A universally conserved arginine
694 residue is highlighted in red. The conserved RGAIS residues in *Leishmania* PKAR3 proteins
695 and the human AI sequence are underlined. **(C)** CNBD: Underlined is the canonical phosphate
696 binding cassette (PBC) motif FGELAL[ILVM]xxxPRAA (35); residues matching the PBC are
697 in bold black type. Highlighted in blue (asterisks) are residues associated with altered ligand
698 specificity in trypanosomatid PKAR1 (38): the switch from alanine (position 5) in human PKA
699 to glutamate in trypanosomatid and the switch from arginine (position 12) in human PKA to a
700 alanine, valine, serine, threonine, or asparagine in the trypanosomatid PKAR sequences.
701 Orange asterisk indicate a valine residue reported to form part of the trypanosomatid specific
702 hydrophobic pocket. **(D)** Hydrophobic pocket: orange asterisk indicates a residue reported to
703 form part of the *Trypanosoma* specific hydrophobic pocket. Highlighted in orange type is a
704 lysine residue reported to increase affinity to binding synthetic nucleoside analogue 7-cyano-
705 7-deazainosine (38).

706 **Figure 2. Localisations of tagged *L. mexicana* PKAC and PKAR subunits.**

707 Micrographs of cells expressing mNG-tagged PKAC or PKAR subunits. **(A)**
708 mNG::*Lmx*PKAC1 (LmxM.34.4010), **(B)** mNG::*Lmx*PKAC2 (LmxM.34.3960), **(C)** mNG::
709 *Lmx*PKAC3 (LmxM.18.1080), **(D)** *Lmx*PKAR1::mNG (LmxM.13.0160), **(E)**
710 *Lmx*PKAR3::mNG (LmxM.33.2820). Panels in A-E show live promastigotes (left), detergent-
711 extracted promastigote cytoskeletons (middle) and live axenic amastigotes (right). For each
712 sample type a merged fluorescence with phase contrast image is shown, and the combined mNG
713 and Hoechst fluorescence. **(F)** Promastigotes in different stages of the cell cycle, expressing

714 *Lmx*PKAR1::mNG and **(G)** mNG::*Lmx*PKAR3. F, flagella; N, nuclei; N*, dividing nucleus, K,
715 kinetoplasts, nol, nucleolus. Scale bar indicates 5 µm.
716
717 **Figure 3. Localisation dependencies of *L. mexicana* PKAC and PKAR subunits.**
718 **(A)** Measurement of the mNG fluorescent signal intensity across a line though the cell body
719 (cartoon) show a clear edge effect for the majority of mNG::*Lmx*PKAC3 cells (i) (black lines,
720 n = 11; red lines show a minority of cells (n = 3) with a diffuse cell body signal. An edge effect
721 was detected for all measured *Lmx*PKAR3::mNG cells (ii) (n = 12). The edge effect for
722 mNG::*Lmx*PKAC3 was lost following *Lmx*PKAR3 deletion (iii) (n = 10). **(B-E)** Micrographs
723 showing the localisation of mNG-tagged *Lmx*PKAC subunits following deletion of *Lmx*PKAR
724 subunits: **(B)** mNG::*Lmx*PKAC1 *ΔLmxPKAR1*; **(C)** mNG::*Lmx*PKAC2 *ΔLmxPKAR1*; **(D)**
725 mNG::*Lmx*PKAC3 *ΔLmxPKAR1*; **(E)** mNG::*Lmx*PKAC3 *ΔLmxPKAR3*. **(F)** Quantitation of
726 fluorescence signal intensity in cells expressing *Lmx*PKAR3::mNG, mNG::*Lmx*PKAC3 and in
727 cells expressing mNG::*Lmx*PKAC3 following *Lmx*PKAR3 deletion. Measurements were taken
728 at six points along the flagellum and cell body as shown in the cartoon.
729
730 **Figure 4. Pharmacological displacement of *Lmx*PKAC1 signal from the axoneme.**
731 Detergent-extracted promastigote cytoskeletons imaged by fluorescence microscopy: from
732 mNG::*Lmx*PKAC1-expressing cells **(A)** without treatment, **(B)** after treatment with cAMP **(C)**
733 toyocamycin and **(D)** inosine as indicated. Merged micrographs of fluorescence with phase
734 contrast are shown as well as just the mNG fluorescent signal pseudo-coloured in grey. For
735 each compound used, 1 µM and 100 µM concentrations were tested. **(D)** Quantification of the
736 cytoskeleton-associated mNG::*Lmx*PKAC1 signals. Background fluorescence was subtracted
737 from maximum intensity values. Each data point represents one cell. Horizontal bar indicated
738 mean corrected fluorescent intensity. Significance was determined using a paired t-test
739 assuming equal variance. *** represents a p-value < 0.001. n > 50 cell measured for each
740 condition. Scale bar indicates 10 µm.
741
742 **Figure 5. Mutant population motility. (A)** Scatter plot of mean population swim speed and
743 directionality (velocity/speed) of parental controls and null mutants for *Lmx*PKAC and
744 *Lmx*PKAR subunits and of dual knock outs of *Lmx*PKAC1/PKAC2 and *Lmx*PKAC1/PKAR3.
745 Swim speed measurement data from at least three replicates per population. Error bars indicate
746 one standard deviation of the speed and directionality measurements. Raw data with p-values
747 from unpaired t-tests for significance are summarised in Supplementary Table 1. **(B)** Phase

748 contrast micrographs overlaid with real traces of flagellar movement over one beat cycle, from
749 a cell propagating either the (upper) symmetric tip-to-base flagellar wave for forward motility,
750 or (lower) the asymmetric base-to-tip ciliary beat for tumbling/turning. On the right are cartoon
751 summaries of flagellar and ciliary waves with an hollow arrow indicating the direction of cell
752 displacement, and a filled grey arrow indicating direction of wave travel. **(C)** Relative
753 frequencies of the waveforms observed in *ΔLmxPKAC* and *ΔLmxPKAR* mutants and control
754 populations. **(D)** Quantification of flagellar length for *Lmx*PKAC and *Lmx*PKAR null mutants
755 and parental control populations where n > 70 for each population. Mann-Whitney U test for
756 significance of mutant flagellar lengths against parental control measurements.
757
758 **Figure 6. Flagellar wave amplitude and frequency parameters.** Fourier decomposition of
759 the tip-to-base uncoordinated wave attempts of *ΔLmxPKAC1,* and the symmetric flagellar
760 waves of *ΔLmxPKAC2, ΔLmxPKAC3, ΔLmxPKAR1 and ΔLmxPKAR3.* **(A)** Computer-
761 generated beat reconstruction of flagellum movement exemplified for each mutant, highlighting
762 the lack of symmetry in *ΔLmxPKAC1* flagellar movement. **(B-F)** Scatter plots of the dominant
763 beat frequency in hertz (Hz) plotted against beat amplitude in degrees for all *Lmx*PKAC and
764 *Lmx*PKAR null mutant populations (purple diamonds) overlaid with measurements from
765 parental control cells (black filled circles). Each point represents one unit of time observed,
766 where total time and n cells observed are summarised in Table 2.

767 **Legends for Supplementary Figures**
768
769 **Supplementary Figure 1. PKAC and PKAR gene synteny.**
770 Cartoon representation of genomic regions for **(A)** PKAC1 and PKAC2, **(B)** PKAC3, **(C)**
771 PKAR1 and **(D)** PKAR3 in representative kinetoplastida species. Gene annotations taken from
772 TritrypDB release 56. The colour coding represents the open reading frames (ORF) of syntenic
773 genes within each genomic locus. Green shading highlights genes encoding our PKA subunits
774 of interest. Genomic loci are not to scale. Blunt end and pointed end of coloured bars represent
775 the transcription start and end of the ORFs respectively.
776
777 **Supplementary Figure 2. PKAC alignments.**
778 Cartoon representation of the classical protein architecture of *L. mexicana* PKAC subunits
779 compared to the *Homo sapiens* reciprocal best blasts (RBB) of *Lmx*PKAC1 and *Lmx*PKAC3

780 (accessions NP_001362493 and NP_005035 respectively). Protein domains are colour coded
781 and information was sourced by using InterProScan. Binding site: IPR017441, active site:
782 IPR008271, protein kinase domain: IPR000719, AGC-kinase: IPR000961. Protein sequence
783 alignments of the **(B)** N-terminus extension, **(C)** binding domain, and **(D)** catalytic core across
784 representative kinetospastid species. **(E)** C-terminus extension of PKAC3 homologues in
785 comparison to *Lmx*PKAC1 and -C2 sequences. Underlined sequences in green indicated
786 conservation across PKAC1 and -C2 in all representative species. Underlined residues in
787 yellow indicates conservation across all PKAC3 sequences. Underlined residues in light blue
788 indicates the FXXF feature in the AGC-kinase family (51).
789
790 **Supplementary Figure 3. PKAC1, PKAC2 and PKAC3 localisation through the**
791 **promastigote cell division cycle.**
792 Promastigotes in different stages of the cell cycle, expressing **(A)** mNG::PKAC1, **(B)** mNG::
793 PKAC2 and **(C)** PKAC3::mNG. The first column displays merged micrographs of fluorescence
794 of Hoeschst DNA stain (magenta), mNG (green) and phase contrast, centre column shows the
795 mNG fluorescent signal pseudo-coloured in grey with DNA stain and the last column displays
796 mNG fluorescent signal pseudo-coloured in grey. F, flagella; N, nuclei; N*, dividing nucleus,
797 K, kinetoplasts, nol, nucleolus. Scale bar indicates 5 μm.
798
799 **Supplementary Figure 4. Localisations of *Leishmania* PKAC and PKAR subunits tagged**
800 **at opposite end.**
801 Fluorescent signal imaged in live promastigote cells expressing **(A)** PKAC1::mNG
802 (LmxM.34.4010), **(B)** PKAC2::mNG (LmxM.34.3960), **(C)** PKAC3::mNG (LmxM.18.1080),
803 **(D)** mNG::PKAR1 (LmxM.13.0160), **(E)** mNG::PKAR3 (LmxM.33.2820). Micrographs of
804 cells expressing PKAR1::mNG with subsequent deletion of the radial spoke protein encoding
805 genes **(F)** RSP11 (LmxM.09.1530) **(G)** RSP3 (LmxM.27.0520) and **(H)** RSP9 (LmxM.07.0930)
806 with (I) Diagnostic PCR to test for loss of the respective RSP gene in the mutant cell lines.
807 Lanes 1 and 12, DNA ladder; Lanes 2-5, genomic DNA from the parental cell line amplified
808 with primers specific to the indicated ORFs; Lanes 6, 8 and 10, amplification of the PF16 ORF
809 from the genomic DNA of the RSP mutants (PCR positive control); Lanes 7, 9 and 11,
810 diagnostic PCR using genomic DNA from the respective RSP mutant cell line.
811
812 **Supplementary Figure 5**. **PCR validation of knock out mutants.**

813 For all gel layouts, the first panel represents a quality control of the primer pairs, whereby PCR
814 amplification using ORF primers listed in figure were used on the parental control genomic
815 DNA template. Following this, the alternation of PCR amplification of a fragment within PF16
816 locus (LmxM.20.1400) was used as positive control and within the ORF of the target gene of
817 deletion for **(A)** *ΔLmxPKAC3*, *ΔLmxPKA*C2, *ΔLmxPKA*C1, **(B)** *ΔLmxPKAR1*, *ΔLmxPKAR3*.
818 **(C)** double null mutants (i) *ΔLmxPKAC1/LmxPKAC2* and (ii) *ΔLmxPKAC1/LmxPKAR3* and
819 **(D)** *ΔLmxPKAR1* and *ΔLmxPKAR3* on parental cell lines expressing mNG C-terminally fused
820 PKAC subunits. The diagnostic primer sequences were taken from LeishGEdit for all but
821 *Lmx*PKAC1 and *Lmx*PKAC2, where a bespoke primer design was required due to sequence
822 similarity. All primer sequences and expected PCR amplicon sizes are listed in Table 3 of the
823 Methods section.
824
825 **Supplementary Figure 6. Growth curve.**
826 Promastigote cell cultures from *ΔLmxPKAR1, ΔLmxPKAR3, ΔLmxPKAC1, ΔLmxPKAC2* and
827 *ΔLmxPKAC3* alongside parental controls were grown in triplicate flasks from densities $1x10^5$
828 to $1x10^7$ cells/ml. **(A)** Cell culture densities were recorded with the Cell Counter CASY TTT
829 (OMNI life science) in viable cells/ml every 24 hours from 0 hours to 96 hours. **(B)** Alongside
830 every cell count, the cell population pseudo-diametres in µm were recorded and plotted. **(C)**
831 We calculated the doubling time of the triplicate cell cultures for each population from 0 - 24hrs
832 and 24 - 48hrs then took the average, equating to a total of six doubling times for each null
833 mutant population. Error bars in all plots represent standard deviation from the mean.
834
835 **Supplementary Figure 7. Summary p-values for flagellar waveform parameters.**
836 P-values from a Mann-Whitney U test was used to test for significance between waveform
837 parameters derived from mutants and the parental control populations. Significance is indicated
838 by asterisks as follows, *** = $p < 0.001$, ** = $p < 0.005$, * = $p < 0.05$. Datasets analysed include
839 wave amplitude (amp), dominant frequency (Hz), waves per flagellum (w/f) and flagellum
840 length (F-length).
841

842 **References**

843 1. Broadhead R, Dawe HR, Farr H, Griffiths S, Hart SR, Portman N, et al. Flagellar motility
844 is required for the viability of the bloodstream trypanosome. Nature. 2006
845 Mar;440(7081):224–7.

2. Nakachi M, Nakajima A, Nomura M, Yonezawa K, Ueno K, Endo T, et al. Proteomic profiling reveals compartment-specific, novel functions of ascidian sperm proteins. Mol Reprod Dev. 2011;78(7):529–49.

3. Pazour GJ, Agrin N, Leszyk J, Witman GB. Proteomic analysis of a eukaryotic cilium. J Cell Biol. 2005 Jul 4;170(1):103–13.

4. Vasquez SSV, van Dam J, Wheway G. An updated SYSCILIA gold standard (SCGSv2) of known ciliary genes, revealing the vast progress that has been made in the cilia research field. Mol Biol Cell. 2021 Oct 6;mbcE21020089.

5. Lindemann CB, Lesich KA. Flagellar and ciliary beating: the proven and the possible. J Cell Sci. 2010 Feb 15;123(4):519–28.

6. Heale KA, Alisaraie L. C-terminal Tail of β-Tubulin and its Role in the Alterations of Dynein Binding Mode. Cell Biochem Biophys. 2020 Sep 1;78(3):331–45.

7. Heuser T, Raytchev M, Krell J, Porter ME, Nicastro D. The dynein regulatory complex is the nexin link and a major regulatory node in cilia and flagella. J Cell Biol. 2009 Dec 14;187(6):921–33.

8. Nlend MC, Schmid A, Sutto Z, Ransford GA, Conner GE, Fregien N, et al. Calcium-mediated, purinergic stimulation and polarized localization of calcium-sensitive adenylyl cyclase isoforms in human airway epithelia. FEBS Lett. 2007 Jul 10;581(17):3241–6.

9. Chung JJ, Miki K, Kim D, Shim SH, Shi HF, Hwang JY, et al. CatSperζ regulates the structural continuity of sperm Ca2+ signaling domains and is required for normal fertility. eLife. 6:e23082.

10. Balbach M, Beckert V, Hansen JN, Wachten D. Shedding light on the role of cAMP in mammalian sperm physiology. Mol Cell Endocrinol. 2018 Jun 15;468:111–20.

11. Alonso CAI, Osycka-Salut CE, Castellano L, Cesari A, Di Siervi N, Mutto A, et al. Extracellular cAMP activates molecular signalling pathways associated with sperm capacitation in bovines. Mol Hum Reprod. 2017 Aug 1;23(8):521–34.

12. ISHIJIMA S. Ca2+ and cAMP regulations of microtubule sliding in hyperactivated motility of bull spermatozoa. Proc Jpn Acad Ser B Phys Biol Sci. 2015 Mar 11;91(3):99–108.

13. Aoki F, Sakai S, Kohmoto K. Regulation of flagellar bending by cAMP and Ca2+ in hamster sperm. Mol Reprod Dev. 1999;53(1):77–83.

14. Roles of cAMP in regulating microtubule sliding and flagellar bending in demembranated hamster spermatozoa. FEBS Lett. 2006 Feb 20;580(5):1515–20.

15. Beltrán C, Zapata O, Darszon A. Membrane potential regulates sea urchin sperm adenylylcyclase. Biochemistry. 1996 Jun 11;35(23):7591–8.

16. Vacquier VD, Loza-Huerta A, García-Rincón J, Darszon A, Beltrán C. Soluble Adenylyl Cyclase of Sea Urchin Spermatozoa. Biochim Biophys Acta. 2014 Dec;1842(12 0 0):2621–8.

884 17. Tash JS. Protein phosphorylation: The second messenger signal transducer of flagellar
885 motility. Cell Motil. 1989;14(3):332–9.

886 18. Hyams JS, Borisy GG. Isolated Flagellar Apparatus Of Chlamydomonas:
887 Characterization Of Forward Swimming And Alteration Of Waveform And Reversal Of
888 Motion By Calcium Ions In Vitro. Journal of Cell Science. 1978 Oct;33(1):235-253.

889 19. Saegusa Y, Yoshimura K. cAMP controls the balance of the propulsive forces generated
890 by the two flagella of Chlamydomonas. Cytoskelet Hoboken NJ. 2015 Aug;72(8):412–21.

891 20. Schmidt JA, Eckert R. Calcium couples flagellar reversal to photostimulation in
892 Chlamydomonas reinhardtii. Nature. 1976 Aug;262(5570):713–5.

893 21. Lodh S, Yano J, Valentine MS, Van Houten JL. Voltage-gated calcium channels of
894 Paramecium cilia. J Exp Biol. 2016 Oct 1;219(Pt 19):3028–38.

895 22. Differential regulation of Paramecium ciliary motility by cAMP and cGMP. J Cell Biol.
896 1988 May 1;106(5):1615–23.

897 23. Nasir A, Richter PR, Le Bail A, Daiker V, Stoltze J, Prasad B, et al. Molecular Cross-
898 Talk between Gravity- and Light-Sensing Mechanisms in Euglena gracilis. Int J Mol Sci.
899 2022 Jan;23(5):2776.

900 24. Mukhopadhyay AG, Dey CS. Reactivation of flagellar motility in demembranated
901 Leishmania reveals role of cAMP in flagellar wave reversal to ciliary waveform. Sci Rep.
902 2016 Nov 16;6(1):37308.

903 25. Mukhopadhyay A, Dey C. Role of calmodulin and calcineurin in regulating flagellar
904 motility and wave polarity in Leishmania. Parasitol Res. 2017 Sep 7;116.

905 26. Schmid A, Bai G, Schmid N, Zaccolo M, Ostrowski LE, Conner GE, et al. Real-time
906 analysis of cAMP-mediated regulation of ciliary motility in single primary human airway
907 epithelial cells. J Cell Sci. 2006 Oct 15;119(20):4176–86.

908 27. Ma W, Silberberg SD, Priel Z. Distinct Axonemal Processes Underlie Spontaneous and
909 Stimulated Airway Ciliary Activity. J Gen Physiol. 2002 Dec;120(6):875–85.

910 28. Christensen ST, Guerra C, Wada Y, Valentin T, Angeletti RH, Satir P, et al. A Regulatory
911 Light Chain of Ciliary Outer Arm Dynein in Tetrahymena thermophila. J Biol Chem.
912 2001 Jan 1;276(23):20048–54.

913 29. Brokaw CJ, Kamiya R. Bending patterns of Chlamydomonas flagella: IV. Mutants with
914 defects in inner and outer dynein arms indicate differences in dynein arm function. Cell
915 Motil. 1987;8(1):68–75.

916 30. Kutomi O, Hori M, Ishida M, Tominaga T, Kamachi H, Koll F, et al. Outer Dynein Arm
917 Light Chain 1 Is Essential for Controlling the Ciliary Response to Cyclic AMP in
918 Paramecium tetraurelia. Eukaryot Cell. 2012 May;11(5):645–53.

919 31. Hamasaki T, Barkalow K, Richmond J, Satir P. cAMP-stimulated phosphorylation of an
920 axonemal polypeptide that copurifies with the 22S dynein arm regulates microtubule

921 translocation velocity and swimming speed in Paramecium. Proc Natl Acad Sci U S A.
922 1991 Sep 15;88(18):7918–22.

923 32. Ardito F, Giuliani M, Perrone D, Troiano G, Muzio LL. The crucial role of protein
924 phosphorylation in cell signaling and its use as targeted therapy (Review). Int J Mol Med.
925 2017 Aug;40(2):271–80.

926 33. Anand GS, Hotchko M, Brown SHJ, Ten Eyck LF, Komives EA, Taylor SS. R-subunit
927 Isoform Specificity in Protein Kinase A: Distinct Features of Protein Interfaces in PKA
928 Types I and II by Amide H/2H exchange Mass Spectrometry. J Mol Biol. 2007 Nov
929 23;374(2):487–99.

930 34. Torres-Quesada O, Mayrhofer JE, Stefan E. The many faces of compartmentalized PKA
931 signalosomes. Cell Signal. 2017 Sep;37:1–11.

932 35. Peng M, Aye TT, Snel B, van Breukelen B, Scholten A, Heck AJR. Spatial Organization
933 in Protein Kinase A Signaling Emerged at the Base of Animal Evolution. J Proteome Res.
934 2015 Jul 2;14(7):2976–87.

935 36. Salathe M. Regulation of Mammalian Ciliary Beating. Annu Rev Physiol.
936 2007;69(1):401–22.

937 37. Cheng Y, Zhang Y, McCammon JA. How does activation loop phosphorylation modulate
938 catalytic activity in the cAMP-dependent protein kinase: A theoretical study. Protein Sci
939 Publ Protein Soc. 2006 Apr;15(4):672–83.

940 38. Bachmaier S, Volpato Santos Y, Kramer S, Githure GB, Klöckner T, Pepperl J, et al.
941 Nucleoside analogue activators of cyclic AMP-independent protein kinase A of
942 Trypanosoma. Nat Commun. 2019 Dec;10(1):1421.

943 39. Shalaby T, Liniger M, Seebeck T. The regulatory subunit of a cGMP-regulated protein
944 kinase A of Trypanosoma brucei. Eur J Biochem. 2001;268(23):6197–206.

945 40. Oberholzer M, Langousis G, Nguyen H, Saada E, Shimogawa M, Jónsson Z, et al.
946 Independent Analysis of the Flagellum Surface and Matrix Proteomes Provides Insight
947 into Flagellum Signaling in Mammalian-infectious Trypanosoma brucei. Mol Cell
948 Proteomics MCP. 2011 Jun 19;10:M111.010538.

949 41. Beneke T, Demay F, Hookway E, Ashman N, Jeffery H, Smith J, et al. Genetic dissection
950 of a Leishmania flagellar proteome demonstrates requirement for directional motility in
951 sand fly infections. Hill KL, editor. PLOS Pathog. 2019 Jun 26;15(6):e1007828.

952 42. Bachmaier S, Witztum R, Tsigankov P, Koren R, Boshart M, Zilberstein D. Protein
953 kinase A signaling during bidirectional axenic differentiation in Leishmania. Int J
954 Parasitol. 2016 Feb;46(2):75–82.

955 43. Dean S, Sunter JD, Wheeler RJ. TrypTag.org: A Trypanosome Genome-wide Protein
956 Localisation Resource. Trends Parasitol. 2017 Feb;33(2):80–2.

957 44. Billington K, Halliday C, Madden R, Dyer P, Barker AR, Moreira-Leite FF, et al.
958 Genome-wide subcellular protein map for the flagellate parasite Trypanosoma brucei. Nat
959 Microbiol. 2023 Mar;8(3):533–47.

960 45. Fort C, Bonnefoy S, Kohl L, Bastin P. Intraflagellar transport is required for the
961 maintenance of the trypanosome flagellum composition but not its length. J Cell Sci. 2016
962 Aug 1;129(15):3026–41.

963 46. Siman-Tov MM, Aly R, Shapira M, Jaffe CL. Cloning from Leishmania major of a
964 developmentally regulated gene, c-lpk2, for the catalytic subunit of the cAMP-dependent
965 protein kinase. Mol Biochem Parasitol. 1996 May;77(2):201–15.

966 47. Kobe B, Kajava AV. The leucine-rich repeat as a protein recognition motif. Curr Opin
967 Struct Biol. 2001 Dec;11(6):725–32.

968 48. Amos B, Aurrecoechea C, Barba M, Barreto A, Basenko EY, Bażant W, et al.
969 VEuPathDB: the eukaryotic pathogen, vector and host bioinformatics resource center.
970 Nucleic Acids Res. 2022 Jan 7;50(D1):D898–911.

971 49. Steinberg RA, Cauthron RD, Symcox MM, Shuntoh H. Autoactivation of Catalytic (Co)
972 Subunit of Cyclic AMP-Dependent Protein Kinase by Phosphorylation of Threonine 197.
973 Mol Cell Biol. :10.

974 50. Steichen JM, Kuchinskas M, Keshwani MM, Yang J, Adams JA, Taylor SS. Structural
975 Basis for the Regulation of Protein Kinase A by Activation Loop Phosphorylation. J Biol
976 Chem. 2012 Apr 27;287(18):14672–80.

977 51. Etchebehere LC, Bemmelen MXPV, Anjard C, Traincard F, Assemat K, Reymond C, et
978 al. The Catalytic Subunit of Dictyostelium cAMP-Dependent Protein Kinase. Eur J
979 Biochem. 1997;248(3):820–6.

980 52. Chan TO, Armen RS, Yadav S, Shah S, Zhang J, Tiegs BC, et al. A tripartite cooperative
981 mechanism confers resistance of the protein kinase A catalytic subunit to
982 dephosphorylation. J Biol Chem. 2020 Mar;295(10):3316–29.

983 53. Tsigankov P, Gherardini PF, Helmer-Citterich M, Späth GF, Myler PJ, Zilberstein D.
984 Regulation Dynamics of Leishmania Differentiation: Deconvoluting Signals and
985 Identifying Phosphorylation Trends. Mol Cell Proteomics MCP. 2014 Jul;13(7):1787–99.

986 54. Jäger AV, De Gaudenzi JG, Mild JG, Cormack BM, Pantano S, Altschuler DL, et al.
987 Identification of novel cyclic nucleotide binding proteins in Trypanosoma cruzi. Mol
988 Biochem Parasitol. 2014 Dec;198(2):104–12.

989 55. Fischer Weinberger R, Bachmaier S, Dandugudumula R, Phan IQ, Almoznino M, Githure
990 GB, et al. A divergent protein kinase A in the human pathogen *Leishmania* is associated
991 with developmental morphogenesis [Internet]. Cell Biology; 2021 Apr [cited 2021 May
992 19]. Available from: http://biorxiv.org/lookup/doi/10.1101/2021.04.24.440790

993 56. Poteet-Smith CE, Shabb JB, Francis SH, Corbin JD. Identification of Critical
994 Determinants for Autoinhibition in the Pseudosubstrate Region of Type Iα cAMP-
995 dependent Protein Kinase. J Biol Chem. 1997 Jan;272(1):379–88.

996 57. Scott JD, Fischer EH, Demaille JG, Krebs EG. Identification of an Inhibitory Region of
997 the Heat-Stable Protein Inhibitor of the cAMP-Dependent Protein Kinase. Proc Natl Acad
998 Sci U S A. 1985;82(13):4379–83.

58. Banky P, Huang LJ, Taylor SS. Dimerization/docking domain of the type Ialpha regulatory subunit of cAMP-dependent protein kinase. Requirements for dimerization and docking are distinct but overlapping. J Biol Chem. 1998 Dec 25;273(52):35048–55.

59. Wheeler RJ, Gluenz E, Gull K. The cell cycle of Leishmania: morphogenetic events and their implications for parasite biology. Mol Microbiol. 2011 Feb;79(3):647-62.

60. Baker N, Catta-Preta CMC, Neish R, Sadlova J, Powell B, Alves-Ferreira EVC, Geoghegan V, Carnielli JBT, Newling K, Hughes C, Vojtkova B, Anand J, Mihut A, Walrad PB, Wilson LG, Pitchford JW, Volf P, Mottram JC. Systematic functional analysis of Leishmania protein kinases identifies regulators of differentiation or survival. Nat Commun. 2021 Feb 23;12(1):1244.

61. Halliday C, Billington K, Wang Z, Madden R, Dean S, Sunter JD, et al. Cellular landmarks of Trypanosoma brucei and Leishmania mexicana. Mol Biochem Parasitol. 2019 Jun;230:24–36.

62. Gaillard AR, Diener DR, Rosenbaum JL, Sale WS. Flagellar Radial Spoke Protein 3 Is an a-Kinase Anchoring Protein (Akap). J Cell Biol. 2001 Apr 16;153(2):443–8.

63. Yang C, Yang P. The Flagellar Motility of Chlamydomonas pf25 Mutant Lacking an AKAP-binding Protein Is Overtly Sensitive to Medium Conditions. Mol Biol Cell. 2006 Jan;17(1):227–38.

64. Gaillard AR, Fox LA, Rhea JM, Craige B, Sale WS. Disruption of the A-kinase anchoring domain in flagellar radial spoke protein 3 results in unregulated axonemal cAMP-dependent protein kinase activity and abnormal flagellar motility. Mol Biol Cell. 2006 Jun;17(6):2626–35.

65. Pigino G, Ishikawa T. Axonemal radial spokes. Bioarchitecture. 2012 Feb 1;2(2):50–8.

66. Dahlin HR, Zheng N, Scott JD. Beyond PKA: Evolutionary and structural insights that define a docking and dimerization domain superfamily. J Biol Chem. 2021 Aug;297(2):100927.

67. Sivadas P, Dienes JM, St Maurice M, Meek WD, Yang P. A flagellar A-kinase anchoring protein with two amphipathic helices forms a structural scaffold in the radial spoke complex. J Cell Biol. 2012 Nov 12;199(4):639–51.

68. Zhang J, Xu J, Li H, Zhang Y, Ma Z, Bechthold A, et al. Enhancement of toyocamycin production through increasing supply of precursor GTP in Streptomyces diastatochromogenes 1628. J Basic Microbiol. 2022 Jun;62(6):750–9.

69. Boitz JM, Ullman B, Jardim A, Carter NS. Purine salvage in Leishmania: complex or simple by design? Trends Parasitol. 2012 Aug;28(8):345–52.

70. Walker BJ, Ishimoto K, Wheeler RJ. Automated identification of flagella from videomicroscopy via the medial axis transform. Sci Rep. 2019 Mar 21;9(1):5015.

71. Walker BJ, Wheeler RJ, Ishimoto K, Gaffney EA. Boundary behaviours of Leishmania mexicana: A hydrodynamic simulation study. J Theor Biol. 2019 Feb;462:311–20.

1037 72. Edwards BFL, Wheeler RJ, Barker AR, Moreira-Leite FF, Gull K, Sunter JD. Direction
1038 of flagellum beat propagation is controlled by proximal/distal outer dynein arm
1039 asymmetry. Proc Natl Acad Sci. 2018 Jul 31;115(31):E7341–50.

1040 73. Wang Z, Beneke T, Gluenz E, Wheeler RJ. The single flagellum of Leishmania has a
1041 fixed polarisation of its asymmetric beat. J Cell Sci. 2020 Oct 22;133(20):jcs246637.

1042 74. Gadelha C, Wickstead B, Gull K. Flagellar and ciliary beating in trypanosome motility.
1043 Cell Motil. 2007;64(8):629–43.

1044 75. Świeżawska B, Duszyn M, Jaworski K, Szmidt-Jaworska A. Downstream Targets of
1045 Cyclic Nucleotides in Plants. Front Plant Sci. 2018 Oct 1;9:1428.

1046 76. Regulation of 22S dynein by a 29-kD light chain. J Cell Biol. 1994 Aug 1;126(3):727–35.

1047 77. Berman HM, Eyck LFT, Goodsell DS, Haste NM, Kornev A, Taylor SS. The cAMP
1048 binding domain: An ancient signaling module. Proc Natl Acad Sci. 2005 Jan 4;102(1):45–
1049 50.

1050 78. Lefièvre L, Jha KN, Lamirande E de, Visconti PE, Gagnon C. Activation of Protein
1051 Kinase A During Human Sperm Capacitation and Acrosome Reaction. J Androl.
1052 2002;23(5):709–16.

1053 79. Soriano-Úbeda C, Romero-Aguirregomezcorta J, Matás C, Visconti PE, García-Vázquez
1054 FA. Manipulation of bicarbonate concentration in sperm capacitation media improves in
1055 vitro fertilisation output in porcine species. J Anim Sci Biotechnol. 2019 Mar
1056 11;10(1):19.

1057 80. Beneke T, Madden R, Makin L, Valli J, Sunter J, Gluenz E. A CRISPR Cas9 high-
1058 throughput genome editing toolkit for kinetoplastids. R Soc Open Sci. 2017
1059 May;4(5):170095.

1060 81. Collins TJ. ImageJ for microscopy. BioTechniques. 2007 Jul;43(1S):S25–30.

1061 82. Schindelin J, Arganda-Carreras I, Frise E, Kaynig V, Longair M, Pietzsch T, et al. Fiji: an
1062 open-source platform for biological-image analysis. Nat Methods. 2012 Jul;9(7):676–82.

1063 83. Wheeler RJ. Use of chiral cell shape to ensure highly directional swimming in
1064 trypanosomes. PLOS Comput Biol. 2017 Jan 31;13(1):e1005353.

1065 84. Walker BJ, Wheeler RJ. High-speed multifocal plane fluorescence microscopy for three-
1066 dimensional visualisation of beating flagella. J Cell Sci. 2019 Aug 15;132(16):jcs231795.

1067

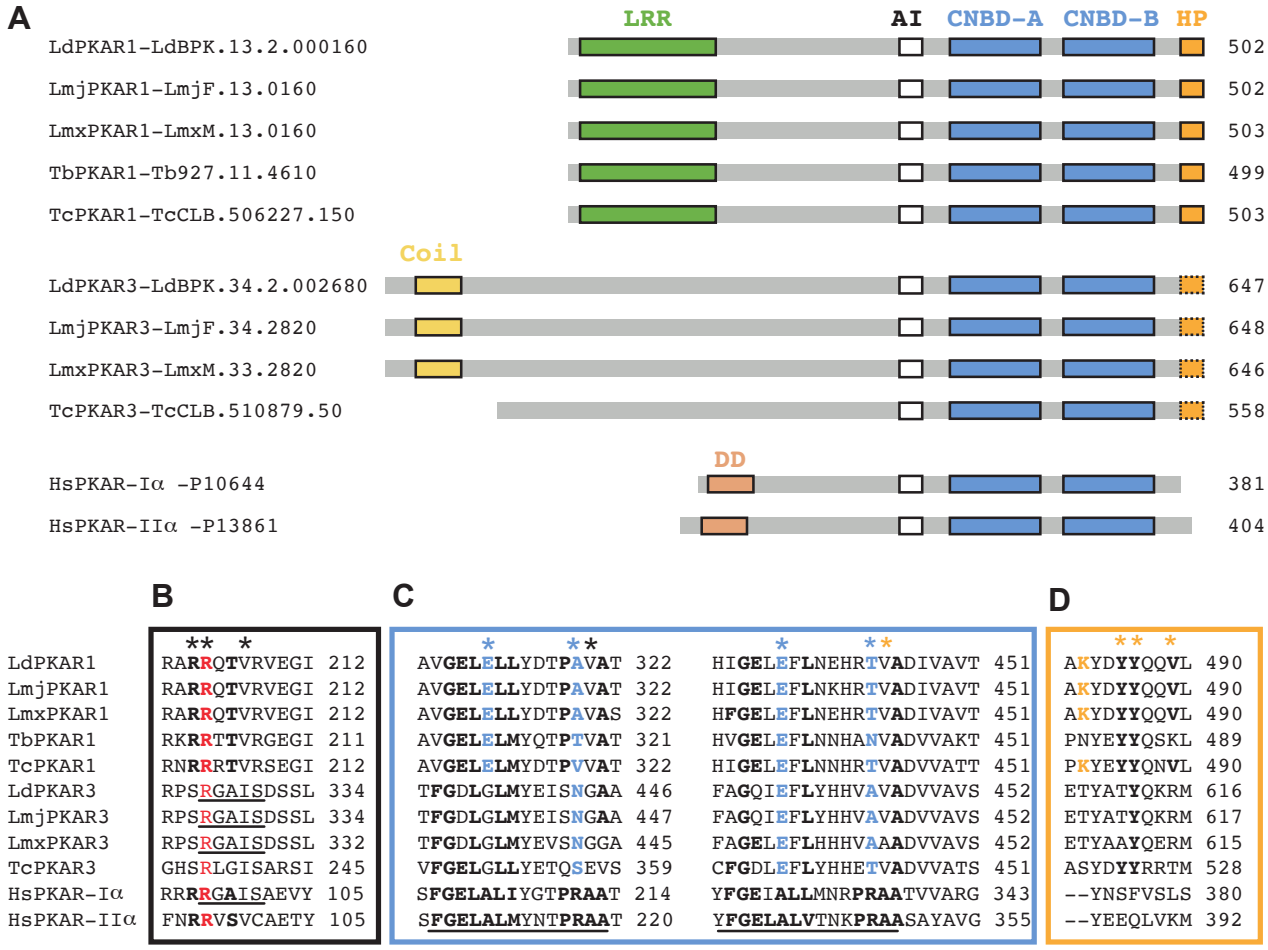
A
LRR
AI
CNBD-A
CNBD-B
HP
LdPKAR1-LdBPK.13.2.000160 502
LmjPKAR1-LmjF.13.0160 502
LmxPKAR1-LmxM.13.0160 503
TbPKAR1-Tb927.11.4610 499
TcPKAR1-TcCLB.506227.150 503
Coil
LdPKAR3-LdBPK.34.2.002680 647
LmjPKAR3-LmjF.34.2820 648
LmxPKAR3-LmxM.33.2820 646
TcPKAR3-TcCLB.510879.50 558
DD
HsPKAR-Iα -P10644 381
HsPKAR-IIα -P13861 404
B
C
D
LdPKAR1 RARRQTVRVEGI 212 AVGELELLYDTPAVAT 322 HIGELEFLNEHRTVADIVAVT 451 AKYDYYQQVL 490
LmjPKAR1 RARRQTVRVEGI 212 AVGELELLYDTPAVAT 322 HIGELEFLNKHRTVADIVAVT 451 AKYDYYQQVL 490
LmxPKAR1 RARRQTVRVEGI 212 AVGELELLYDTPAVAS 322 HFGELEFLNEHRTVADIVAVT 451 AKYDYYQQVL 490
TbPKAR1 RKRRTTVRGEGI 211 AVGELELMYQTPTVAT 321 HVGELEFLNNHANVADVVAKT 451 PNYEYYQSKL 489
TcPKAR1 RNRRRTVRSEGI 212 AVGELELMYDTPVVAT 322 HIGELEFLNNHRTVADVVATT 451 PKYEYYQNVL 490
LdPKAR3 RPSRGAISDSSL 334 TFGDLGLMYEISNGAA 446 FAGQIEFLYHHVAVADVVAVS 452 ETYATYQKRM 616
LmjPKAR3 RPSRGAISDSSL 334 TFGDLGLMYEISNGAA 447 FAGQIEFLYHHVAVADVVAVS 452 ETYATYQKRM 617
LmxPKAR3 RPSRGAISDSSL 332 TFGDLGLMYEVSNGGA 445 FAGELEFLHHHVAAADVVAVS 452 ETYAAYQERM 615
TcPKAR3 GHSRLGISARSI 245 VFGELGLLYETQSEVS 359 CFGDLEFLYHHETVADVVATS 451 ASYDYYRRTM 528
HsPKAR-Iα RRRRGAISAEVY 105 SFGELALIYGTPRAAT 214 YFGEIALLMNRPRAATVVARG 343 --YNSFVSLS 380
HsPKAR-IIα FNRRVSVCAETY 105 SFGELALMYNTPRAAT 220 YFGELALVTNKPRAASAYAVG 355 --YEEQLVKM 392

Figure 1

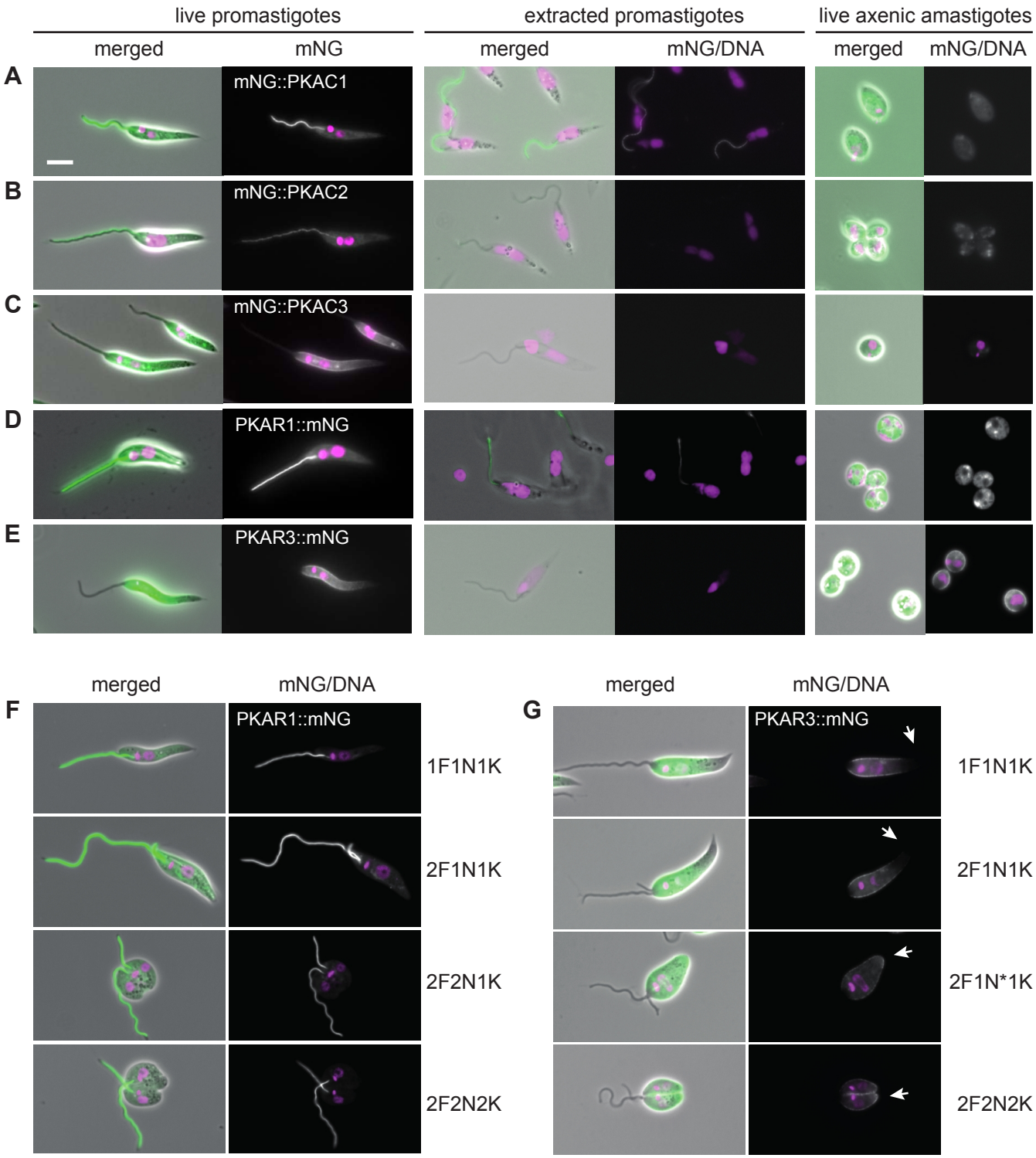
live promastigotes
extracted promastigotes
live axenic amastigotes
merged
mNG
merged
mNG/DNA
merged
mNG/DNA
A
mNG::PKAC1
B
mNG::PKAC2
C
mNG::PKAC3
D
PKAR1::mNG
E
PKAR3::mNG
merged
mNG/DNA
F
PKAR1::mNG
1F1N1K
2F1N1K
2F2N1K
2F2N2K
merged
mNG/DNA
G
PKAR3::mNG
1F1N1K
2F1N1K
2F1N*1K
2F2N2K

Figure 2

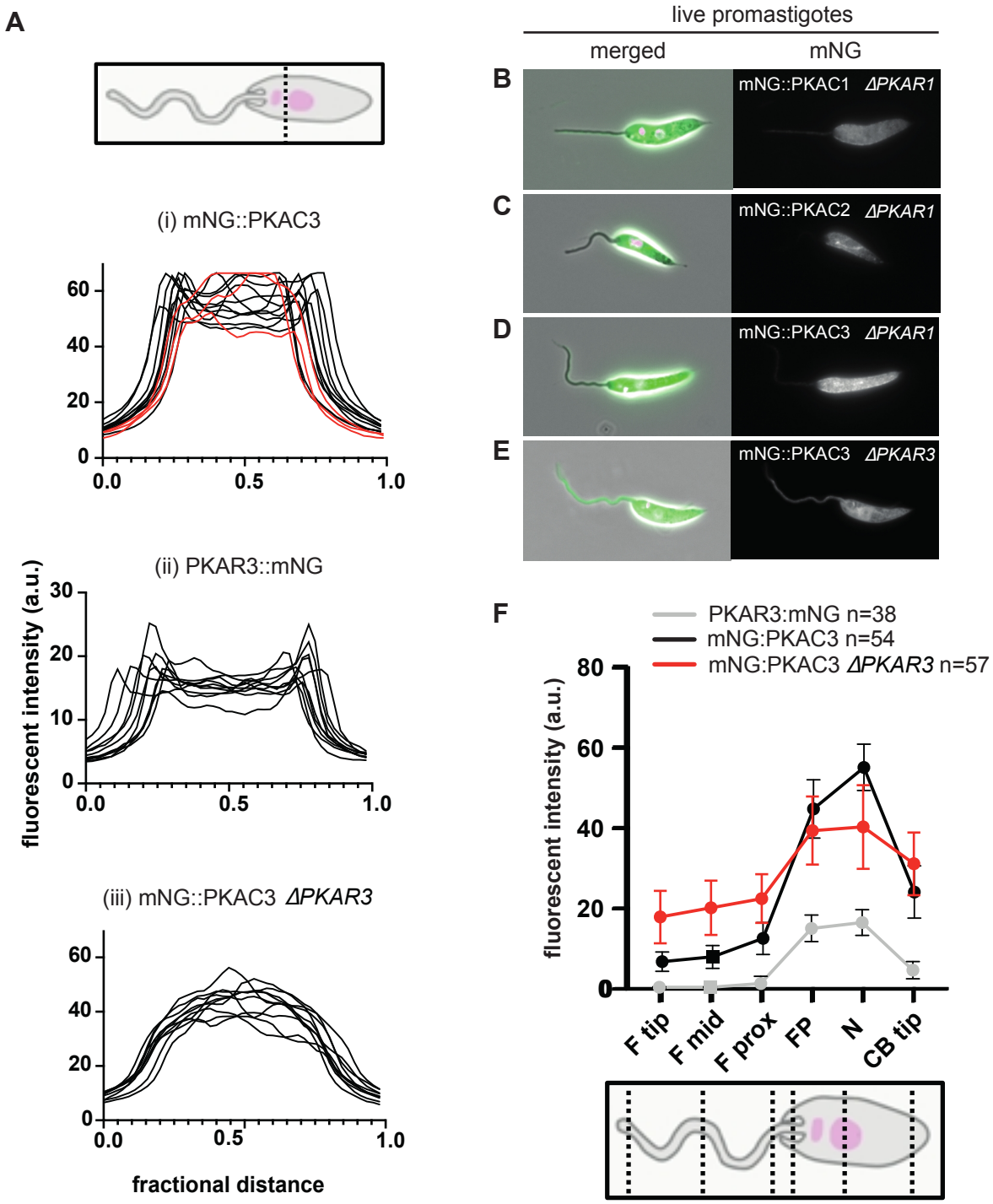
A
(i) mNG::PKAC3
(ii) PKAR3::mNG
(iii) mNG::PKAC3 ΔPKAR3
fluorescent intensity (a.u.)
fractional distance
live promastigotes
merged
mNG
B
mNG::PKAC1 ΔPKAR1
C
mNG::PKAC2 ΔPKAR1
D
mNG::PKAC3 ΔPKAR1
E
mNG::PKAC3 ΔPKAR3
F
PKAR3:mNG n=38
mNG:PKAC3 n=54
mNG:PKAC3 ΔPKAR3 n=57
F tip
F mid
F prox
FP
N
CB tip

Figure 3

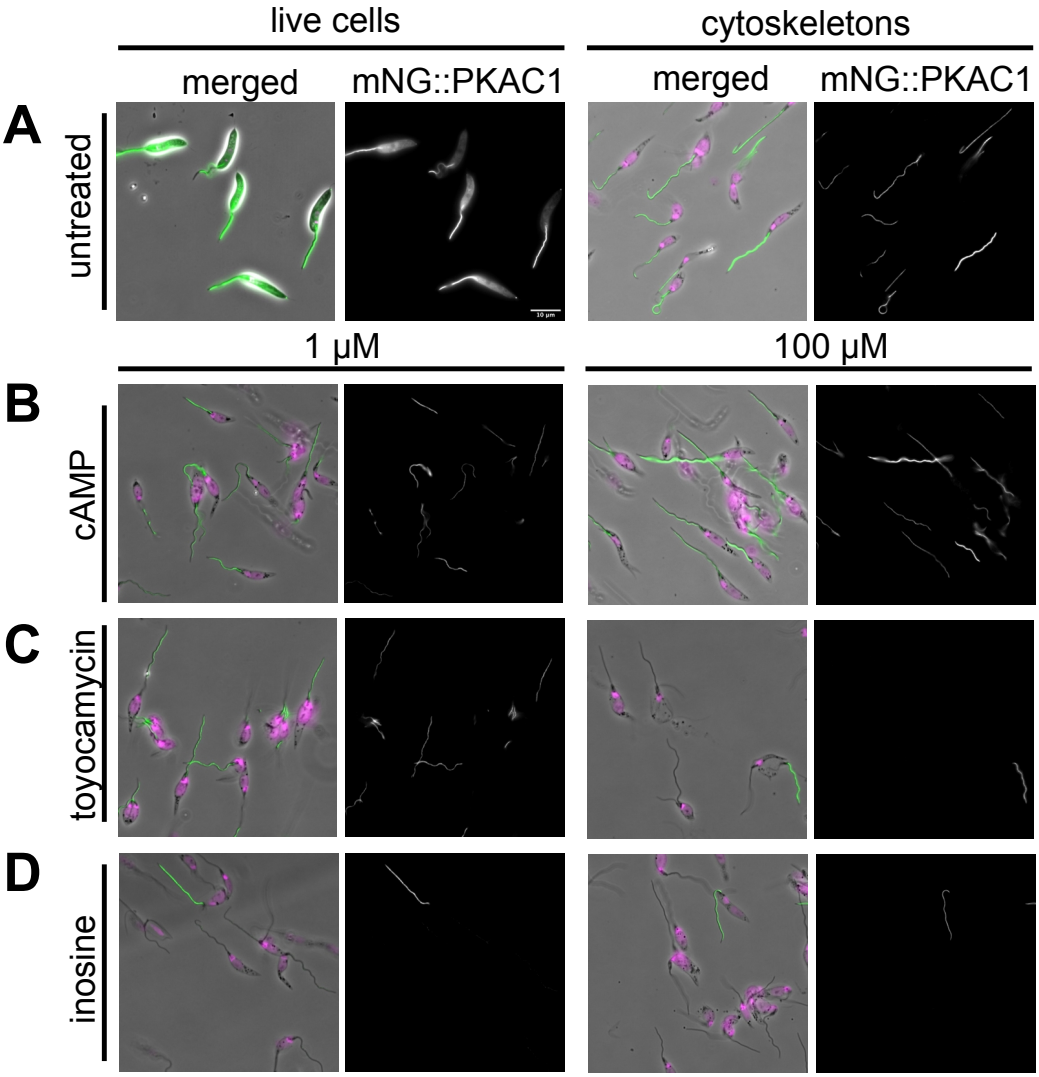
live cells
cytoskeletons
merged
mNG::PKAC1
merged
mNG::PKAC1
A
untreated
1 μM
100 μM
B
cAMP
C
toyocamycin
D
inosine

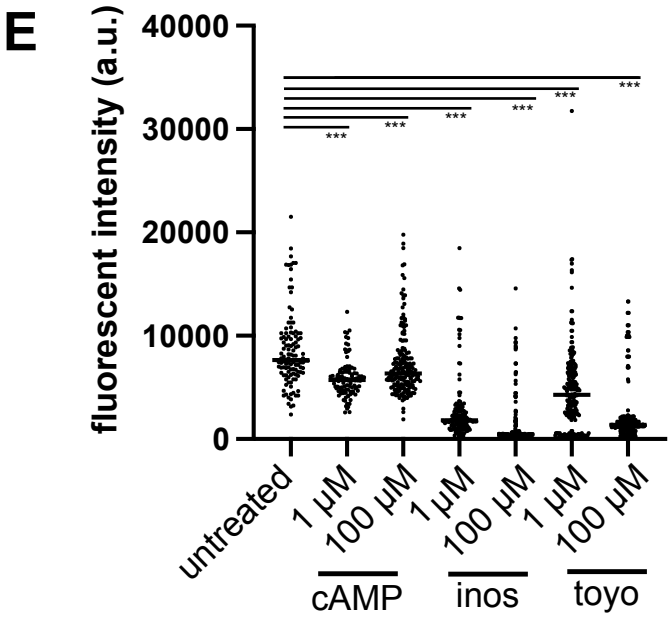
E
fluorescent intensity (a.u.)
40000
30000
20000
10000
0
untreated
1 μM
100 μM
1 μM
100 μM
1 μM
100 μM
cAMP
inos
toyo

Figure 4

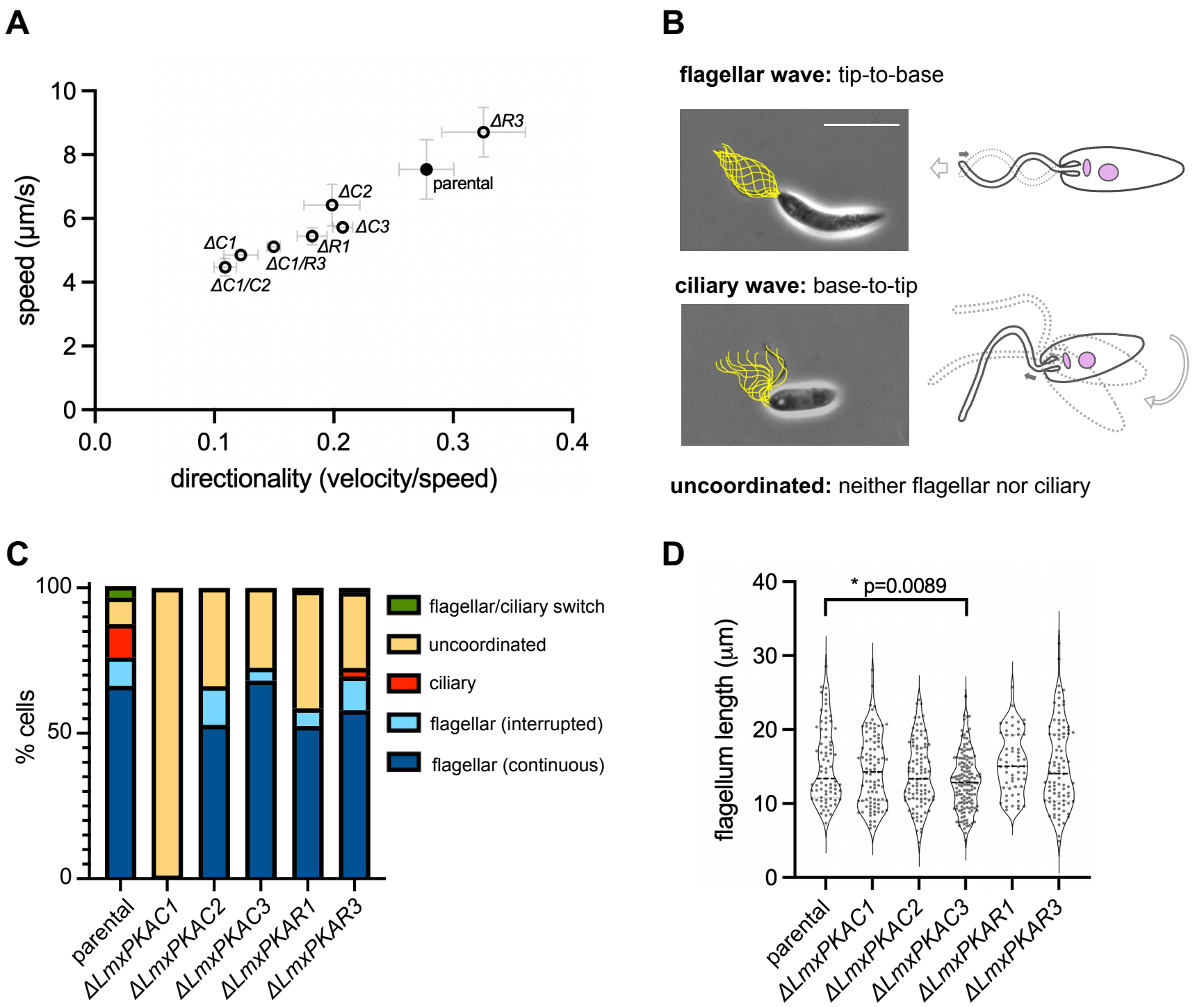
A
speed (µm/s)
directionality (velocity/speed)
ΔR3
parental
ΔC2
ΔC3
ΔR1
ΔC1
ΔC1/R3
ΔC1/C2
B
flagellar wave: tip-to-base
ciliary wave: base-to-tip
uncoordinated: neither flagellar nor ciliary
C
% cells
flagellar/ciliary switch
uncoordinated
ciliary
flagellar (interrupted)
flagellar (continuous)
parental
ΔLmxPKAC1
ΔLmxPKAC2
ΔLmxPKAC3
ΔLmxPKAR1
ΔLmxPKAR3
D
flagellum length (µm)
* p=0.0089
parental
ΔLmxPKAC1
ΔLmxPKAC2
ΔLmxPKAC3
ΔLmxPKAR1
ΔLmxPKAR3

Figure 5

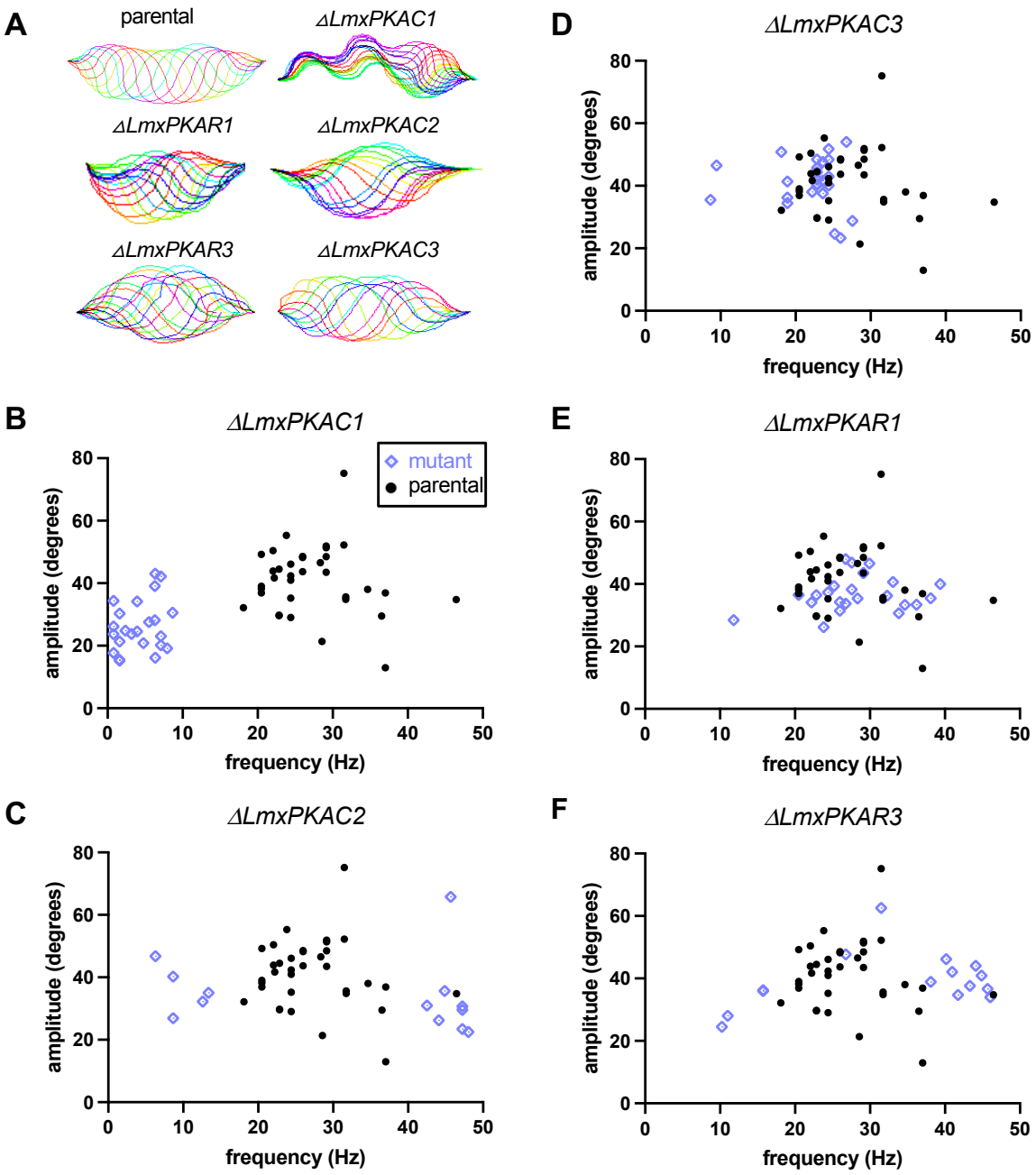
A
parental
ΔLmxPKAC1
ΔLmxPKAR1
ΔLmxPKAC2
ΔLmxPKAR3
ΔLmxPKAC3
B
ΔLmxPKAC1
mutant
parental
amplitude (degrees)
frequency (Hz)
C
ΔLmxPKAC2
D
ΔLmxPKAC3
E
ΔLmxPKAR1
F
ΔLmxPKAR3

Figure 6

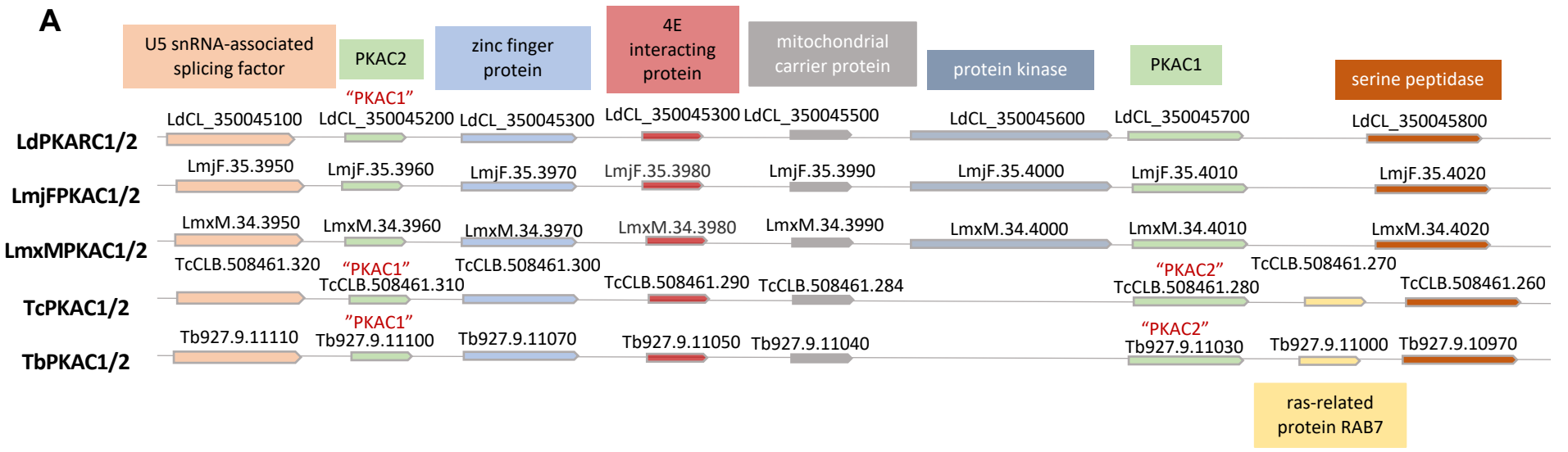

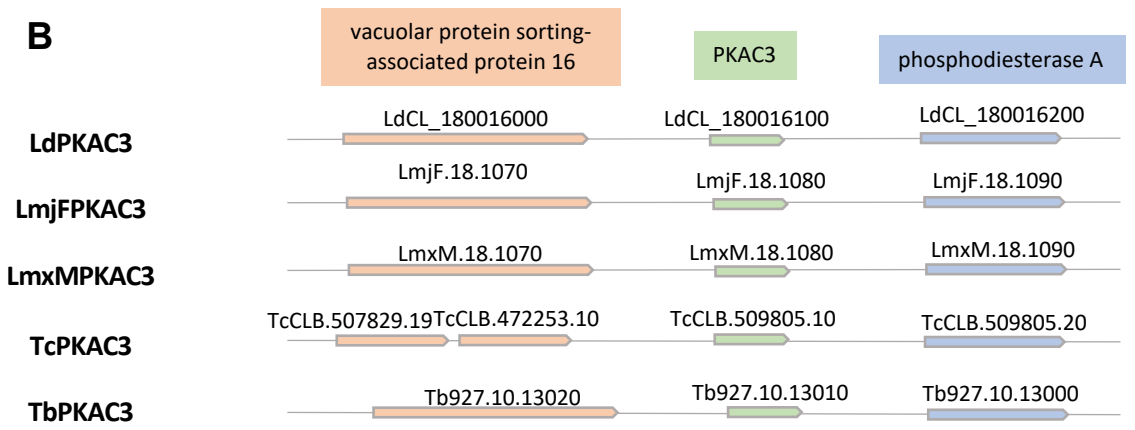

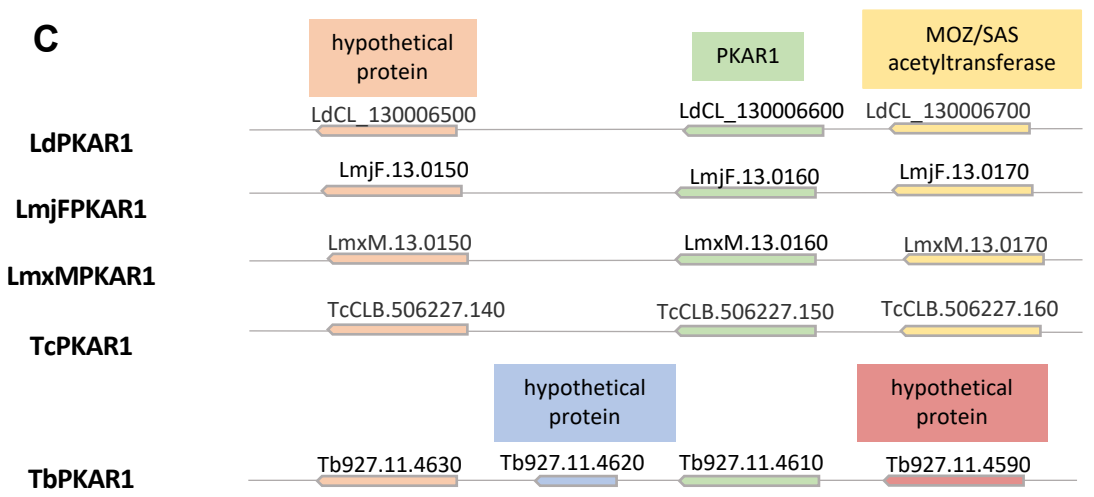

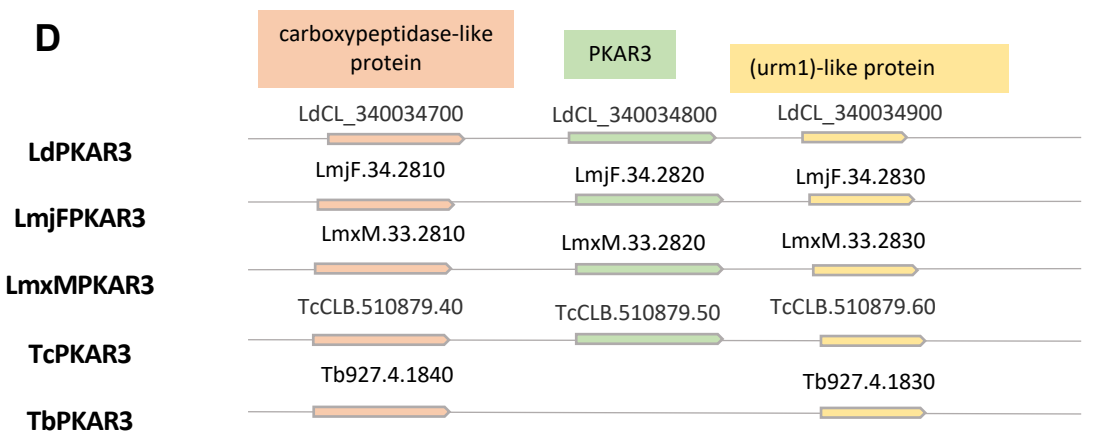

Supplementary Figure 1

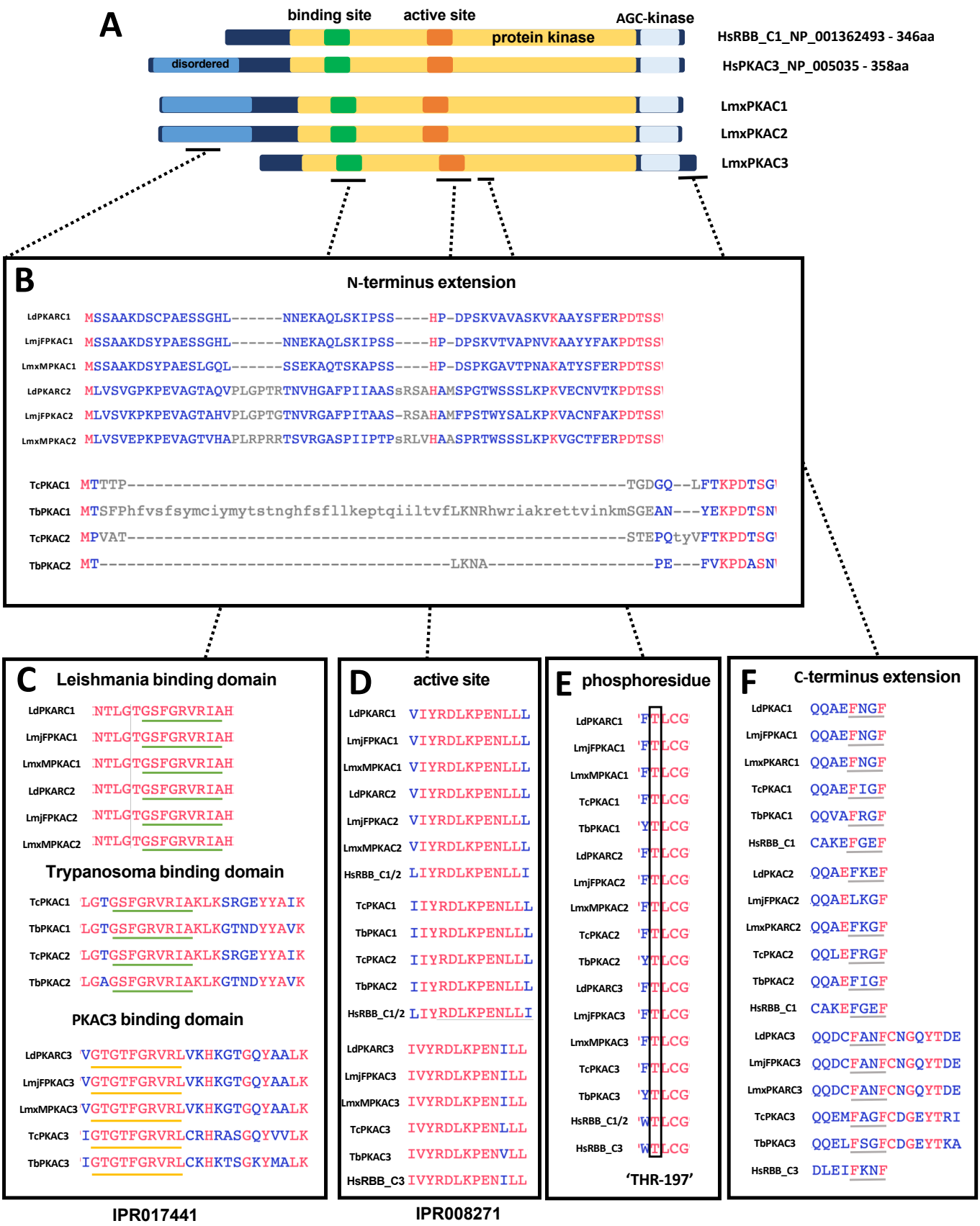

Supplementary Figure 2

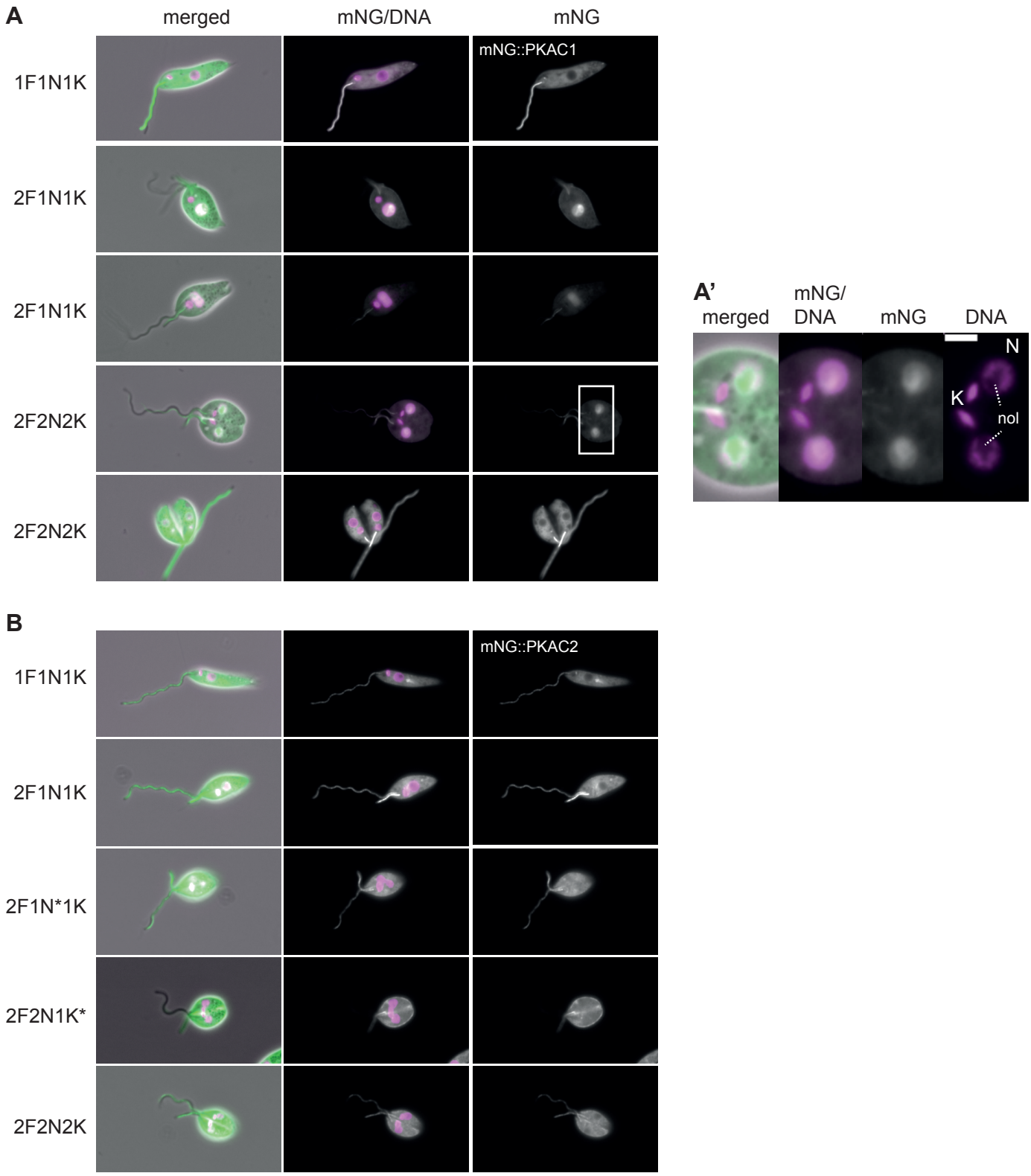

Supplementary Figure 3

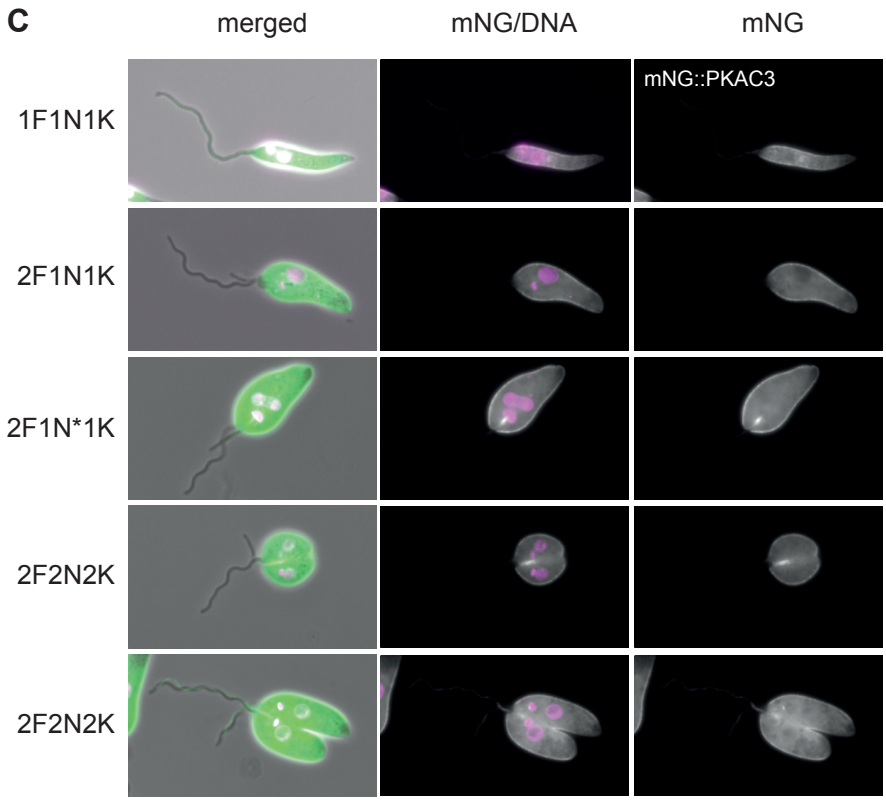

Supplementary Figure 3

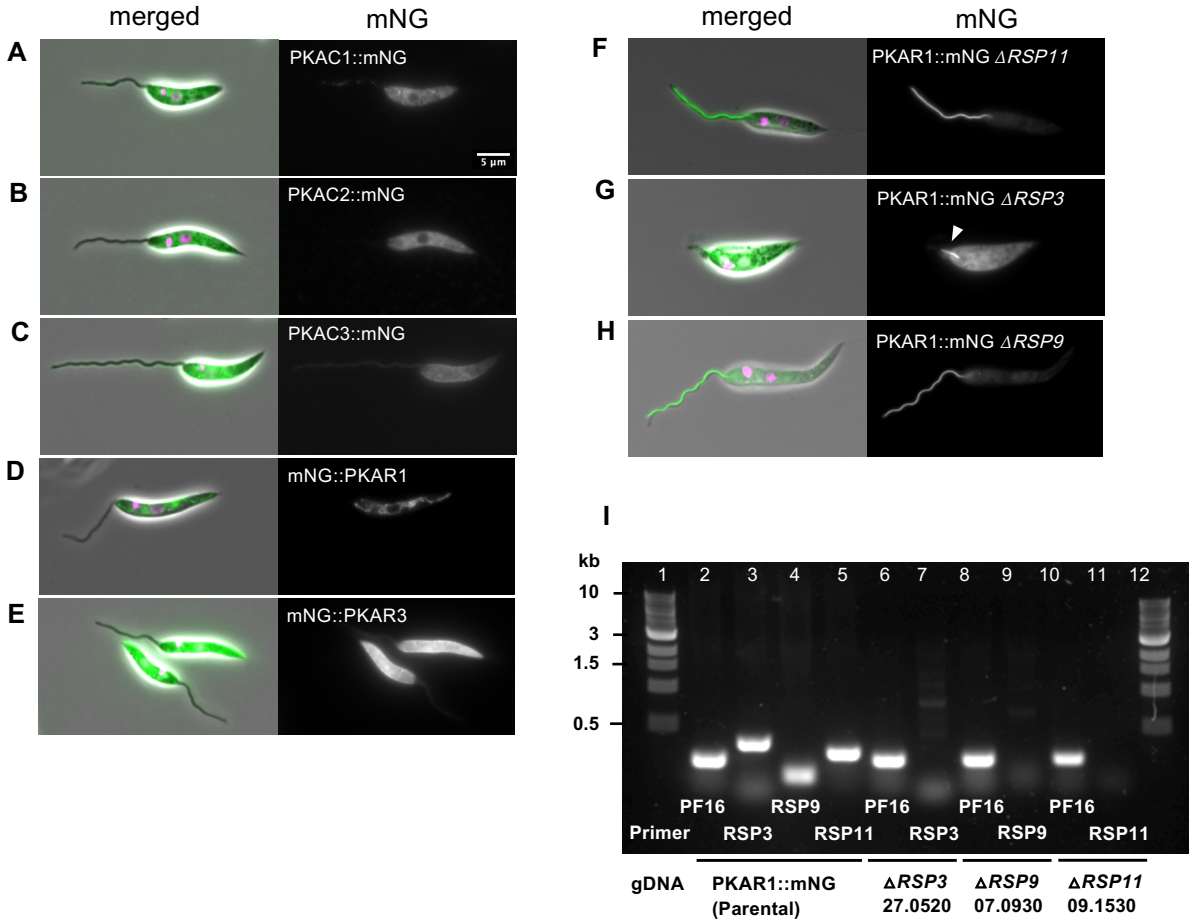

Supplementary Figure 4

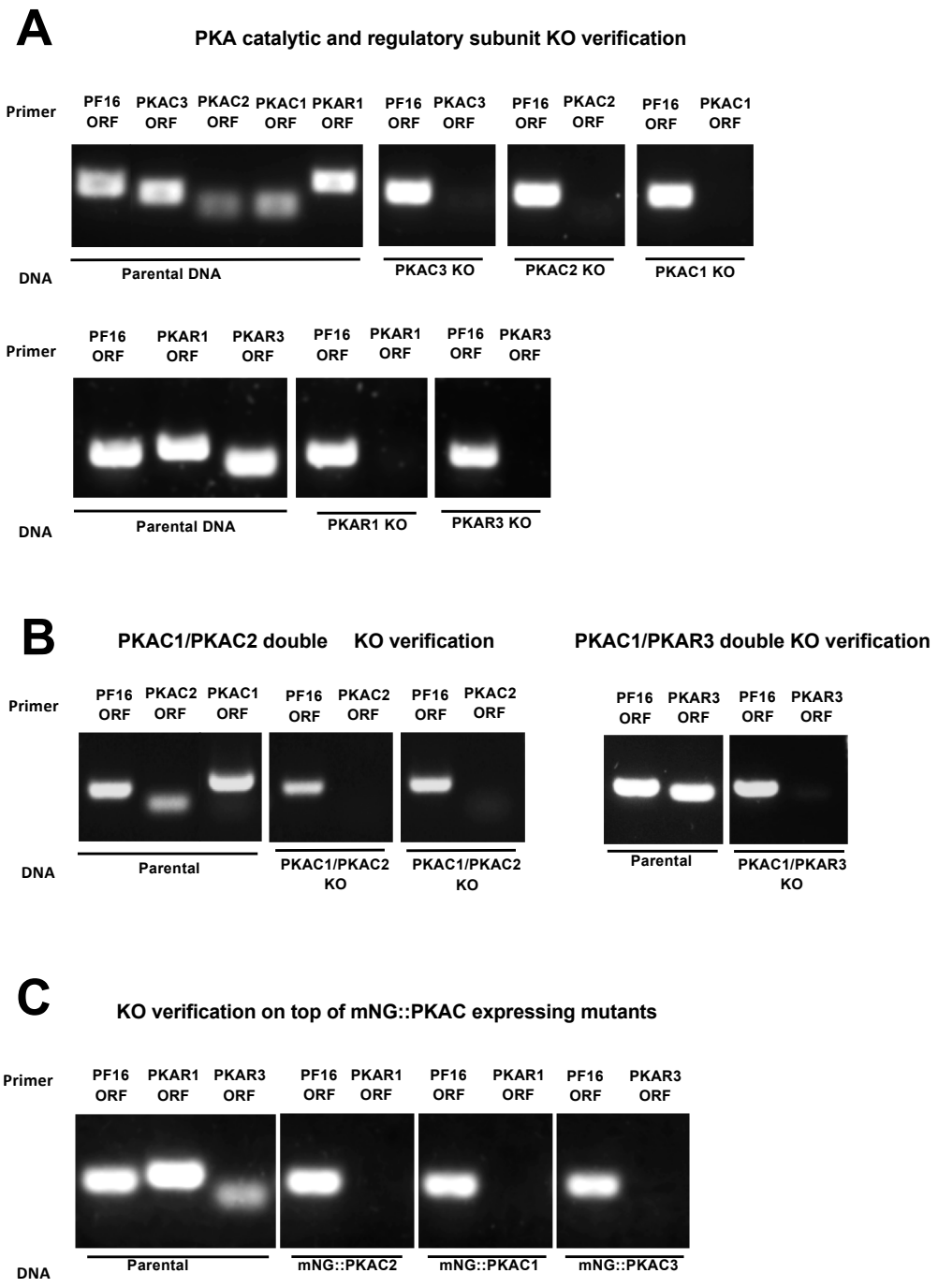

Supplementary Figure 5

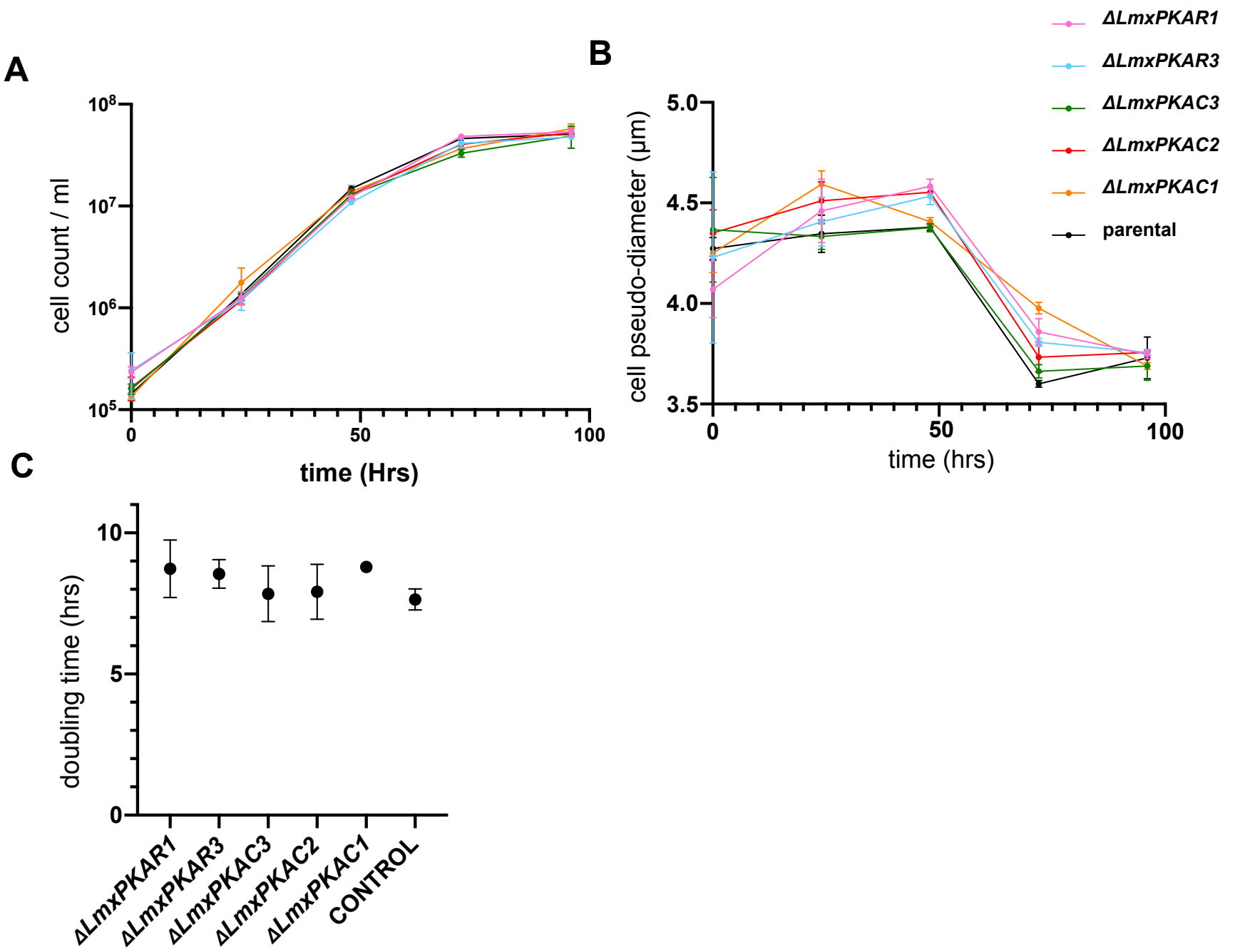

Supplementary Figure 6

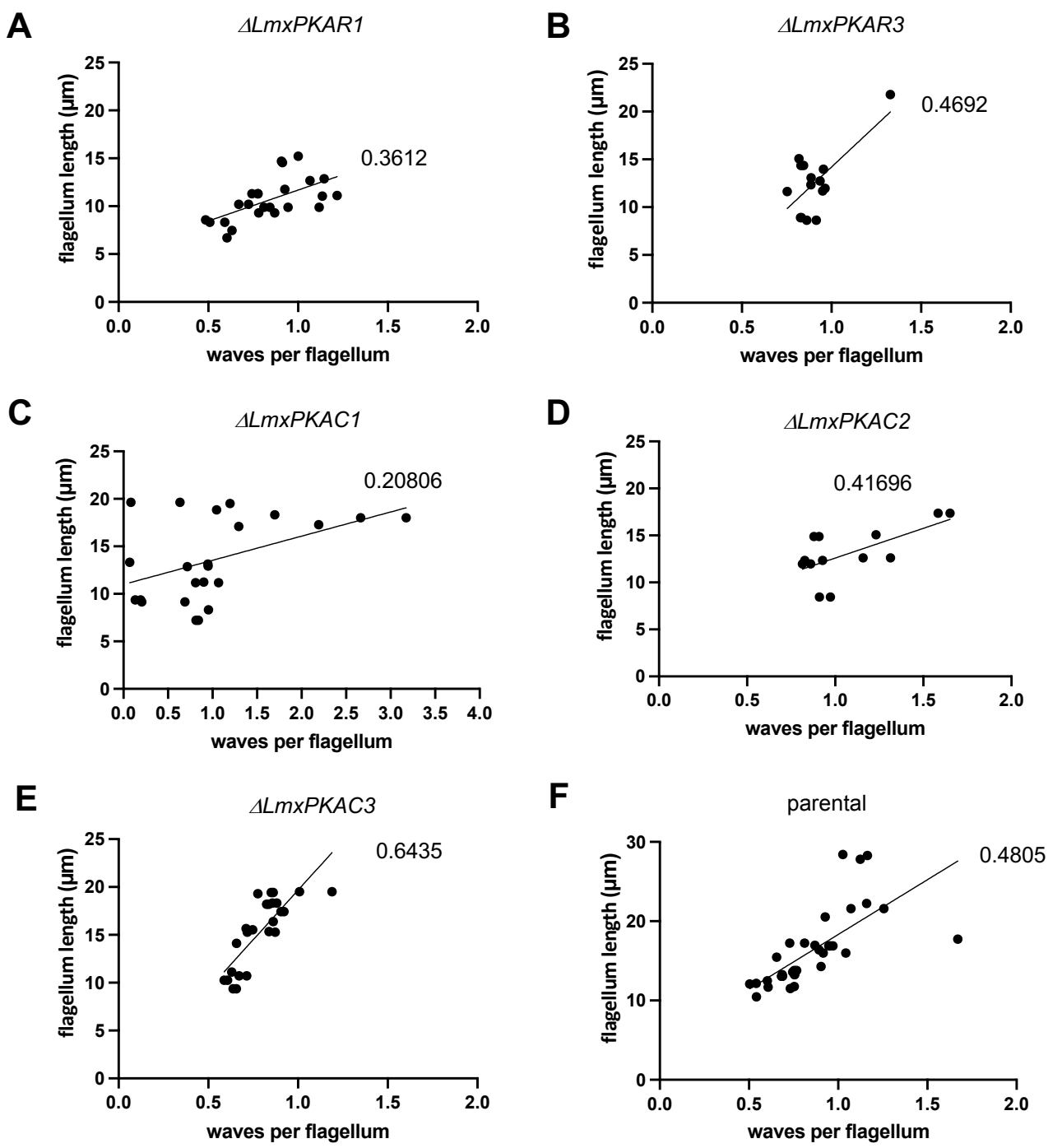

Supplementary Figure 7

Supplementary Table 2. Waveform parameters from mutants and the parental control populations were compared with a Mann-Whitney U test. The table shows the p-values, with significance indicated by asterisks as follows, *** = p < 0.001, ** = p < 0.005, * = p < 0.05. Datasets analysed include wave amplitude, dominant frequency (Hz), waves per flagellum (w/f) and flagellum length (F-length).

	ΔLmxPKAR1	***ΔLmxPKAR3***	***ΔLmxPKAC1***	***ΔLmxPKAC2***	***ΔLmxPKAC3***
amplitude	0.0538	0.3556	*** <0.001	* 0.0178	0.9881
frequency	0.2564	0.0551	*** <0.001	0.2659	** 0.0035
w/f	0.9664	0.2048	0.5357	* 0.0093	0.3456
F-length	0.4636	0.7211	0.4434	0.1858	* 0.0089